Review Article

Nano Research
2023, 16(7): 8570–8595

ISSN 1998-0124 CN 11-5974/O4
https://doi.org/10.1007/s12274-022-5307-1

Two-dimensional covalent organic frameworks for electrocatalysis: Achievements, challenges, and opportunities

Ruoyu Zhao[1,§], Teng Wang[2,§], Junjun Li[1], Yongxia Shi[1], Man Hou[1], Yong Yang[2] (✉), Zhicheng Zhang[1] (✉), and Shengbin Lei[1] (✉)

[1] *Department of Chemistry, School of Science & Tianjin Key Laboratory of Molecular Optoelectronic Sciences, Tianjin University, Tianjin 300072, China*

[2] *State Key Laboratory of Solidification Processing, Center of Advanced Lubrication and Seal Materials, Northwestern Polytechnical University, Xi'an 710072, China*

[§] *Ruoyu Zhao and Teng Wang contributed equally to this work.*

Received: 18 October 2022 / **Revised:** 6 November 2022 / **Accepted:** 7 November 2022

ABSTRACT

Covalent organic frameworks (COFs) represent an emerging class of crystalline porous polymers with high porosity, good stability, and adjustable structure, and their excellent characteristics lay a solid foundation for electrocatalysis. This review systematically introduces the design principles of the catalytic sites in two-dimensional (2D) COF-based electrocatalysts and analyzes the relationship between 2D COF structure and their electrocatalytic performances. In particular, the recent progress in the field of 2D COFs as electrocatalysts is comprehensively summarized. Finally, we discuss the current shortcomings and challenges on tailoring 2D COF for high-performance electrocatalysts in details, and look forward to promoting more researches on 2D COF-based electrocatalysts.

KEYWORDS

covalent organic frameworks, electrocatalysts, two-dimensional, active centers

1 Introduction

In the past hundred years, the combustion of fossil fuels has promoted the process of global industrialization and the rapid development of society. However, the greenhouse gases released by the burning of fossil fuels not only caused the melting of glaciers, but also led to extremely low temperatures and blizzards in various regions in 2020, which is closely related to the polar vortex derived from global warming [1, 2]. While the unabated fossil-fuel consumption caused enormous public-health hazards [3]. Therefore, it is imperative to achieve the transition from fossil fuels to clean energies, including water splitting [4–6], fuel cells [7, 8], metal–air batteries [9], and carbon dioxide conversion [10–13]. Searching for a low-energy-consumption, high-selectivity catalyst to accelerate the key conversion reaction has become the research hotspot.

Covalent organic framework (COF) is a framework material composed of light elements (H, B, C, N, and O, etc.) and units connected by covalent bonds, which usually possesses the crystalline and long-ordered networks. Relying on the topological natures of building blocks, COFs are categorized into two-dimensional (2D) COFs [14] and three-dimensional (3D) COFs [15]. Notably, 2D COFs, as a novel class of layer-stacked materials, have attracted considerable interests owing to the following advantages: i) the stacked column and the 2D plane, giving rise to the tailored electron conductivity; ii) the long-ordered structures, contributing to the spatial separation of catalytic sites and preventing agglomeration, thereby significantly improving the electrochemical performances [16]; iii) the high porosity, conducive for the substrate to enter the pores and contact the active center of the reaction; iv) the excellent thermal and chemical stability, ensuring the superior turnover number of the catalyst; v) the adjustable pore size and topological structure built by units with different molecular lengths and shapes, favoring the investigation of catalytic reaction mechanism of different structures. In addition, it has been reported that bubbles may adhere to the electrode surface in the process of gas generation, resulting in hindering the mass transfer process and reducing the catalytic performance [17, 18]. Introducing halogen, alkyl chain, and other functional groups into the 2D COF structure could create a super-hydrophobic surface to solve the bubble problem [19]. Based on the aforementioned discussions, a large number of 2D COFs have been designed as electrocatalysts for clean energies.

Currently, several unique and insightful reviews of COFs for electrocatalytic conversion have been published [19, 20]. However, in this review, we focus on the association between the structural design of materials and their electrocatalytic functions. We firstly introduce the design principles of catalytic sites in 2D COF materials, including heteroatom incorporation, metallization, and encapsulation of active sites in pores. Then, we emphasize how the functions of 2D COF materials affect their electrocatalytic performances, and cover the latest development of 2D COFs in electrochemical conversion. Finally, we discuss the shortcomings and challenges of 2D COF-based electrocatalysts, and propose perspectives for further researches.

Address correspondence to Zhicheng Zhang, zczhang19@tju.edu.cn; Yong Yang, yongyangfj@nwpu.edu.cn; Shengbin Lei, shengbin.lei@tju.edu.cn

2 Materials design for COF-based electrocatalysts

Activity, selectivity and stability are the major factors for the evaluation of electrocatalysts. The identity of the catalytic center plays an important role in the activity and selectivity. Since the electrocatalytic reactions always occur on the active centers, the apparent activity depends on the unit activity of each active center as an intrinsic character and the number of exposed active sites as the extrinsic character. Therefore, incorporating appropriate heteroatom dopants into the COF structure has a decisive effect on the performance of the material. The main methods to create catalytic active centers in framework materials include heteroatom incorporation, metallization, and the encapsulation of active site in the pore.

2.1 Heteroatom incorporation

For COF composed of light elements, especially metal-free COF catalysts, heteroatoms such as N, F, P, and S are the main active sites in the framework, which strongly affect the catalytic activity [21]. It is attributed to the charge polarization of carbon and heteroatoms caused by the difference in electron negativities [22, 23]. Therefore, monomers containing heteroatoms are designed to easily construct non-metallic catalytic active centers in COF materials through a bottom-up approach. Perfluorinated covalent triazine framework (CTF) derivative displayed the better conductivity to CH_4 production with the faradaic efficiency (FE) of 99.3% (Fig. 1(a)) [24]. Electrochemical characterization and density functional theory (DFT) calculations demonstrated that the fluorine covalently bound with nitrogen active sites contributed to the ultrahigh selectivity for CH_4. Doping with heteroatoms could also apply to the oxygen reduction reaction (ORR), Hao et al. constructed the thermalized covalent triazine frameworks (TTFs) with different heating temperatures from 400 to 700 °C (Fig. 1(b)) and found that the ratios of pyridinic (N_i) and pyrrolic nitrogen (N_{ii}) configurations increased with the raise of thermalized temperature, same as the conductivity, while the ratio of quaternary nitrogen (N_{iii}) types fell. Due to the highest conductivity, TTF-700 exbihited the most positive onset potential (E_{onset}) of 0.822 V vs. reversible hydrogen electrode (RHE), and the highest diffusion limiting current density (i_d) of 4.63 mA·cm^{-2}. Further controlling the nitrogen configurations, they observed that the nitrogen configurations affected the performances of ORR and the N_{iii} favored the electrocatalytic activities. Besides, doping with other heteroatoms in the TTF-700, the F-doped catalyst (TTF-F) possessing more positive E_{onset}, half-wave potential, and greater i_d, denotes better catalytic activity; while the B-doped catalyst (TTF-B) has batter catalytic selectivity, manifested as lower HO_2^- yield and higher four-electron selectivity [25]. In another related work, two kinds of COFs with thiophene structure have been exploited for metal-free ORR (Fig. 1(c)). The comparison of linear sweep voltammetry (LSV) curves between thiophene-based COFs and analogous thiophene-free COF verified the efficient catalytic ability derived from the pentacyclic thiophene-sulfur structure [26]. JUC-528 as bithiophene-based COF showed the smallest Tafel slope of 65.9 mV·dec^{-1}, the largest electrochemical double layer capacitance (C_{dl}) value of 7.6 mF·cm^{-2}, and the turnover frequency (TOF) value of 0.00315·s^{-1}, indicating the faster reaction kinetics and the more efficient active site utilization, due to the bigger pore size and greater thiophene content. Therefore, investigating the role of different heteroatoms and their principles is essential to optimize the performance of metal-free catalysts and achieve precise control of the chemical structure of the catalyst.

Currently, COF-based electrocatalytic materials doped with heteroatoms are limited to several methods: monomers design, pyrolysis, and post-synthesis functionalization. It is hoped that more doping methods can be expanded, such as the COF-to-COF conversion strategy [27–30].

2.2 Metallization

Metal is the most frequently chosen active center in catalytic reactions, and the type, distribution, and coordination of the metal determine the efficiency and selectivity of the catalyst. The coordination of metal ions with organic ligands is the basic logic for introducing metal active sites into COF-based electrocatalysts. The modular nature of COF offers an ideal platform that allows the coordination of metal ions with organic building blocks. It is good for the uniform separation and distribution of metal active centers. According to the position of the ligands, the metalization of COF can be grouped in the following different categories: (i) coordination with monomers, (ii) coordination with pendant functional groups, and (iii) coordination with covalent linkers (Fig. 2).

Coordination with monomers is particularly prevalent among the researches of COF-based electrocatalysts. The most popular complex in the field of electrocatalysis is a heterocyclic structure

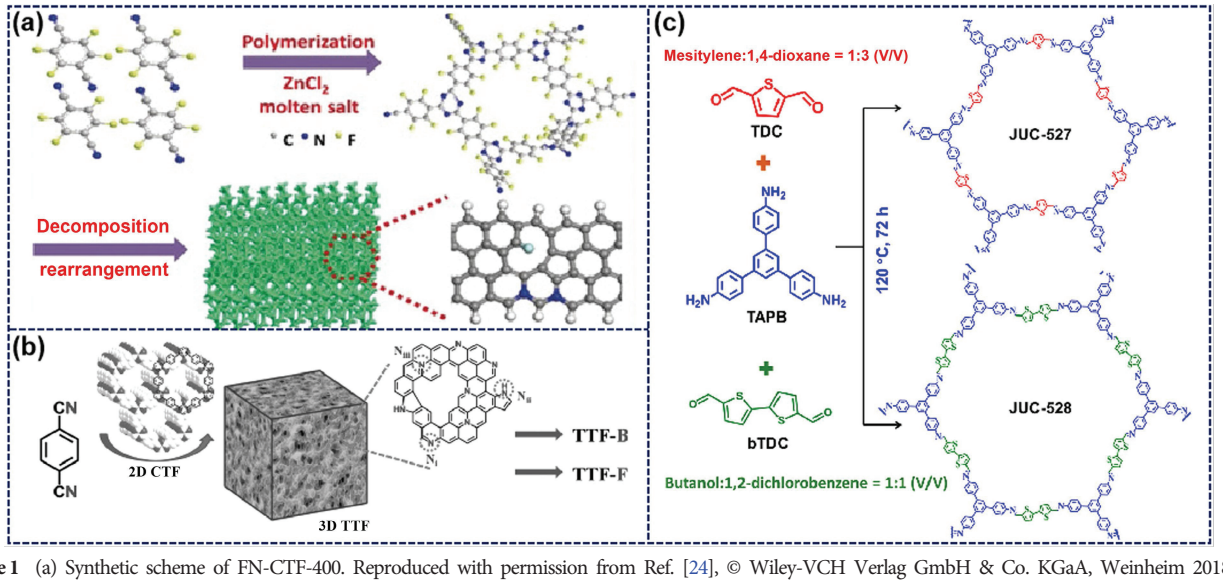

Figure 1 (a) Synthetic scheme of FN-CTF-400. Reproduced with permission from Ref. [24], © Wiley-VCH Verlag GmbH & Co. KGaA, Weinheim 2018. (b) Synthetic scheme of doping TTF. Reproduced with permission from Ref. [25], © WILEY-VCH Verlag GmbH & Co. KGaA, Weinheim 2015. (c) Synthetic scheme of JUC-527 and JUC-528. Reproduced with permission from Ref. [26], © American Chemical Society 2020.

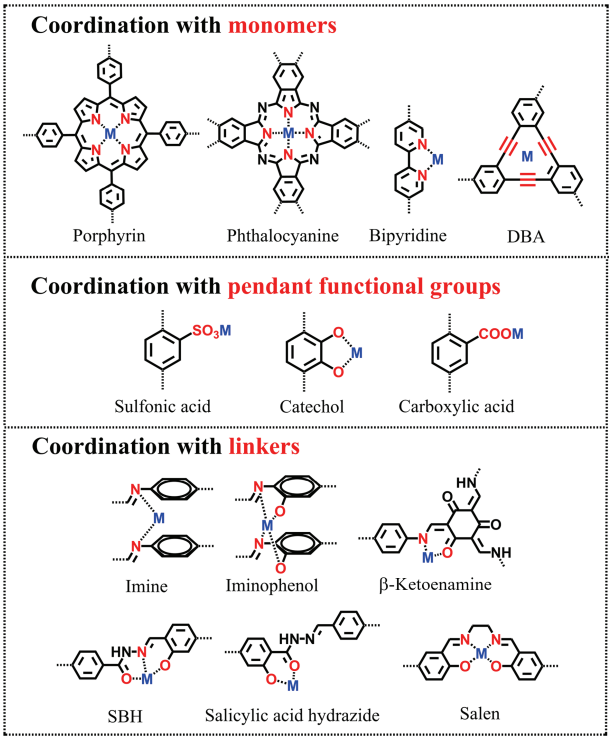

Figure 2 Ligands for the metallization of COFs.

containing four pyrrole subunits, such as porphyrin [31, 32], phthalocyanine [33, 34], etc. The utilization of these macrocyclic monomers is inspired by nature. Metalloporphyrins and their derivatives are usually observed in organelles related to energy transfer and biocatalysis. For example, chlorophyll, an important pigment contained in all organisms capable of photosynthesis, is a magnesium porphyrin derivative; heme, which is a cofactor for enzymes and proteins, is also a ferriporphyrin compound. In addition to porphyrin and phthalocyanine, there are other complexes coordinating with metals, such as bipyridine. Co, Fe, Re, other monometals [35–37], and even bimetals [38, 39] have been introduced into bipyridine-based COF. The porous carbon material through the pyrolysis of Co and Fe bimetallic COF is proved to be a multifunctional electrochemical catalyst, exhibiting excellent performance in ORR, hydrogen evolution reaction (HER), and oxygen evolution reaction (OER) [39]. In addition, a lot of complexes, such as dehydrobenzocyclopentene (DBA) [40] have been reported for the synthesis of 2D COFs, but their application in the field of electrocatalysis deserves further exploration.

Compared with the above-mentioned strategy, coordination with pendant functional groups to achieve metallization is more universal. The pendant functional groups coordinated with metal ions can be obtained following the bottom-up approaches by designing building blocks containing functional groups, or based on dynamic covalent chemistry (DCC), transforming linkers into building blocks containing pendant groups [30], or functionalized after synthesis. In the past few years, some excellent review articles summarized the post-synthesis modification strategy of COF [41–43]. Luo and colleagues successfully immobilized the metal on the sulfonic acid side groups of COF through ion exchange, and synthesized a bimetallic single-site heterogeneous catalyst for OER [44–46]. 2D COF with catechol [47, 48] and carboxylic acid [49] ligands can also be complexed with metal ions, but their electrocatalytic application has been rarely reported until now.

The third method of COF metallization is the complexation of metal ions with COF linkers. Imines are versatile groups for incorporating a variety of active metal species, and imine-linked COFs have a lot of researches, mature synthesis systems, as well as complete reaction mechanisms. As early as 2011, there was an exploration of COF as the catalyst for Suzuki–Miyaura coupling reaction in which metal ion is complexed with imine bond [50]. The two imine nitrogen atoms between adjacent layers of COF with eclipsed layered-sheet arrangement interact with the catalytic center Pd ion. In addition, the imine linker and other substituents on the monomer can form a more stable multidentate ligand, for example, the COF containing iminophenol synthesized by hydroxyterephthalaldehyde and diamine [51], the β-ketoenamine ligand condensated by 1,3,5-triformylphloroglucinol and diamine monomer [52], the salicylaldehyde benzoyl hydrazone (SBH) ligand yielded between 1,3,5-triformylphloroglucinol and terephthalohydrazide [48, 53], and so on. As one of the most important ligands in coordination chemistry, the post-synthetic modification of N,N'-bis(salicylic)ethylenediamine (salen)-based COF can be metalized with Co^{2+}, Mn^{2+}, Cu^{2+}, Ni^{2+}, and Zn^{2+}. Zn (salen)-based COF can also exchange with Co^{2+}, Mn^{2+}, Cr^{2+}, Fe^{2+}, and V^{4+} without alternation of structural integrity and loss in crystallinity. Salen-based COF has served as the efficient catalyst for the Henry's reaction, asymmetric cyanidation of aldehydes, Diels–Alder reaction, alkene epoxidation, cycloaddition, epoxide ring-opening, and related sequential reactions [54–56]. But there is no research on salen-based COF as the electrocatalytic material yet.

2.3 Encapsulate the active site in the hole

Metal nanoparticles (NPs) with a smaller size, leading to a higher surface atom ratio, have the higher catalytic activity, due to more surface atoms as effective catalytically active sites. However, smaller metal NPs are more unstable and tend to aggregate. In the past, polyvinylpyrrolidone (PVP) was often used to modify metal NPs to reduce the surface energy and prevent aggregation. However, with the development of porous crystalline materials, COF with micropores seems to be an ideal platform for encapsulating ultrafine metal particles. In general, the size of metal NPs, which coordinated with heteroatoms in the COF hybrid materials, is much larger than the size of COF's pore [57–59]. It proves that the interaction between COF and metal NPs is weak, so that the pore cannot confine metal into COFs. Therefore, Lu et al. [60] strengthened the combination of metal ions or NPs with COF by the strongly anchored sulfide groups in the pores (Fig. 3(a)), so that the nucleation sites of the NPs were formed inside the cavity, thereby controlling the particle size to about 1.7 nm (Figs. 3(b)–3(d)).

The general operations of embedding the metal NPs in the pores are as follows: Firstly, the metal ions are introduced into the binding site of the COF by immersing the corresponding metal salt solution, and then reduced to a single NP. In the experiment of depositing metal NPs in COF pores, it is necessary to select a suitable solvent to dissolve the metal salt according to the hydrophobicity or hydrophilicity of the COF's pore. In 2012, Aijaz et al. [61] reported the "double solvents" approach for the first time. By adding the metal precursor solution dropwise into the hydrophobic solvent *n*-hexane, a small amount of the aqueous solution goes inside the hydrophilic pores of the metal–organic framework MIL-101 by capillary force. The hydrophobic environment created by *n*-hexane greatly minimizes the deposition of the precursor solution on the surface. Considering that most electrocatalytic reactions occur in aqueous media, it is inevitable for the hydrophilic pores of COF. Therefore, the double solvents method is also of reference significance for the encapsulation of active sites in the pores of COF electrocatalysts. Besides, the choice of reducing agent is also important. Strong reducing agents (such as sodium borohydride) may also reduce

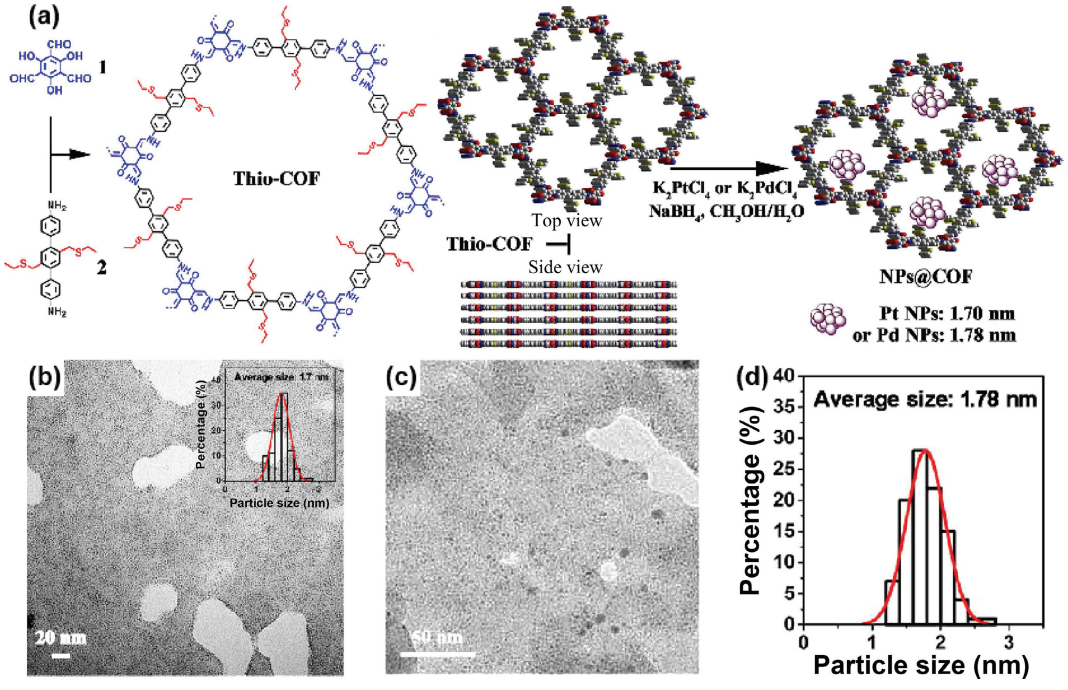

Figure 3 (a) Synthesis and scheme of thio-COF and NPs@COF. (b) Transmission electron microscopy (TEM) image of PtNPs@COF. Inset: the size distribution of Pt NPs. (c) TEM image of PdNPs@COF. (d) The size distribution of Pd NPs. Reproduced with permission from Ref. [60], © American Chemical Society 2017.

the imine linkages of COF, not only metal ions [62] resulting in loss of crystallinity and rigidity, affecting the interaction between the carrier and NPs, even causing the leaching and sintering of the NPs, and reducing the cycle stability of the catalyst. Li et al. [63] reduced palladium ions on the porous organic polymers Pd@CPP-1 (CPP: click-based porous organic polymer) and Pd@CPP-2 through two different pathways, H_2 and $NaBH_4$, respectively. They discovered that palladium NPs reduced by H_2 were evenly distributed in the inner cavities without deposition at the external surface. In contrast, when $NaBH_4$ was chosen, Pd NPs with smaller average diameters were encapsulated within the pores of CPP, while NPs with larger average diameters were deposited on the external surface. On account of the hydrophobicity of aromatic polymers, the author believes that the aqueous solution of $NaBH_4$ cannot be drawn efficiently into the pores by capillary force, and some palladium precursors were redissolved and diffused out of the pores, thereby depositing on the external surface to form large NPs. On the contrary, during H_2 is used, the particle nucleation occurs under solid-phase conditions, and the growth of NPs is restricted by the polymer, resulting in highly dispersed ultrafine palladium NPs. These researches for relevant materials promise to be the instructive role of the active site encapsulation in 2D COFs' holes.

3 Design for the high-activity COF catalysts

As mentioned in Section 2, activity, selectivity, and stability, the most important factors for the evaluation of electrocatalysts, are reflected in COF materials as porosity, conductivity, and stability. Most COFs with high crystallinity exhibit the porosity and surface area comparable to the calculated theoretical values of the single crystal. The conductivity of 2D COFs mainly relies on the two paths of in-plane extended π conjugation and out-of-plane π–π stacking, which fully manifest the importance for the control of structural regularity. Stability is another substantial element to assess electrocatalyst performances. Acidic-pH environment profits HER owing to adequate supplies of protons. Moreover, CO_2 reduction reaction (CO_2RR) performance is typically measured in potassium bicarbonate electrolyte, which ensures the local CO_2 concentration by suppressing the increase of pH near the electrode. Nonetheless, the major product switch shows the pH dependence [64], and CO_2 electrolysis in strong alkali [65] or highly concentrated acid [66] to high-selectivity multi-carbon products has also been realized. Hence the extremely high chemical stability of COF catalysts is the premise to continue the steady performance during long-term electrolysis under harsh conditions.

3.1 Synthesis principles of COFs

In 2005, COF was firstly reported to be synthesized under solvothermal conditions [67]. Currently, this method is still the most conventional synthesis method. Typical protocol is shown as below. Firstly, a Pyrex tube was charged with a mixture of the reactants, solvents, and catalysts. Then it was quickly frozen at 77 K and was sealed to a certain length after vacuuming. After heating at a predetermined temperature for several days, the precipitate was collected, washed, and dried to obtain solid COF powder. High temperature, high pressure, and long reaction time are its obvious shortcomings, although the solvothermal method is universal and applicable to a variety of reactions. Therefore, in recent years, a variety of solvothermal alternatives have been explored, such as microwave [68–71], mechanochemical [72–74], sonochemical [75], and the vapor-assisted conversion method [76, 77].

COF is the rigid macrocyclic framework synthesized by polycondensation reactions. And it is required that the chain growth is driven by covalent bonds and the stacking process of π–π interactions simultaneously in the polymerization of 2D COFs. At present, a lot of researches have been performed on the formation mechanism of boroxine, borate, and imine-linked COF. The crystallization process of borate-linked 2D COF was simulated, tracked, and divided into two steps: nucleation and elongation [78–83]. Unlike boron-containing COF, before the emergence of imine-linked COF, the reaction pathways of imine generation, transimination, and metathesis have been identified in the studies on dynamic covalent chemistry [84]. The two-step mechanism was initially observed with the generation of imine COFs: the rapid formation of the amorphous sediment, followed by dynamic imine exchange and crystallization into the layered

framework [85–87]. Recently, with the improvement of the isolation and activation methods and thorough *in-situ* characterization, it was indicated that crystalline sheets were formed in as short as 60 s, then reorganized and stacked into more ordered structures in a few hours [88]. However, COFs with the boron units have little π electron cloud overlap between the large rings in the plane, the imine-based linkages allow for partially π-conjugated lattices, and the full π conjugation offered by C=C and phenazine bond [89] is more conducive to charge separation, electron transfer, and charge collections. Theoretically, the full π conjugation and long-ordered structure of 2D COFs afford excellent electronic conductivity. Therefore, the mechanistic understanding of the crystallization process for other types of 2D COFs is a worthwhile subject to inform the rational control of polymerization and establish a platform for the high-current-density 2D COF electrocatalysts.

3.2 Design of the linkage

2D COFs are required the long-term stability for the practical electrolysis, and the linkage plays a significant role in supporting the COF structures. Generally, the bonds formed by the higher reversible reactions are weaker, so the corresponding COF materials show the higher crystallinity but lower stability.

Since Yaghi and his colleagues reported the inception of the COFs, i.e., boroxine-linked COF-1 and boronate ester-linked COF-5 in 2005 [67], COFs with plentiful linkages have been developed, possessing different degrees of stability and crystallinity (Fig. 4). The excellent reversibility of the condensations for the boroxine and the boronate ester linkages ensures the high crystallinity products, which are susceptible to skeleton damage in water or even humid air, unsuitable for electrochemical reactions in the presence of aqueous solutions. The triazine [90] and borazine [91] bonds, isostructural with the boroxine linkage, were reported in 2008 and 2012, respectively. Although extremely stable, CTFs were polymerized under severe conditions, such as high temperatures ≥ 400 °C or the catalysis of trifluoromethanesulfonic acid. Even so, it is still difficult to obtain CTFs with crystalline structure. In 2017, the condensation between aldehydes and amidines under mild conditions of ≤ 120 °C and no superacids provided the CTF materials, but did not show any long range crystalline ordering [92]. Subsequently, the *in-situ* alcohol oxidation strategy which controlled the oxidation to aldehyde monomers slowed down the nucleation process and limited the concentration of crystal nuclei. With the precise temperature restraint, the formation of nucleation based on slow oxidation was retarded by the initial low temperature, and the following higher temperature enhanced the crystallinity trend of CTFs, thereby a series of crystalline CTFs were synthesized [93]. Unlike aromatic C=N bonds, employing the Schiff base reactions with higher reactivity, imine-based COFs with the resistance to water and alkaline environments were evolved into the most extensively reported linkages. Similar to imine linkages, the aminal-linked COFs with C–N bonds were reported, as the product of attacking the aldehyde by two secondary amines [94]. Afterwards, an array of related bonds were studied, such as hydrazone [95], β-ketoenamine [96], azine [97], squaraine [98], and indoimine [99]. The above linked-COFs retain the crystallinity in water and aqueous HCl solution. Squaraine, with the zwitterionic structure and electron-deficient skeleton, allowed two-directional electron flow through the periodic columnar π-arrays and over the 2D extended π conjugation. With regard to the hydrazone- and azine-linked COFs, the strong affinity for CO_2 gas [100, 101], the coordination of different metal ions [102, 103], as well as the robustness in water, acid, and base [104–106], show great potential in the catalysis field. β-Ketoenamine-linked COFs are the first example of the conversion and locking of the imine linkages in a cascade fashion. The combination of reversible imine condensation and irreversible tautomerization of enol-to-keto endows the COFs with increased bond stability, which maintains crystallinity after the treatment with boiling water and 9 M HCl for up to 7 days. However, the nonconjugative character of β-ketoenamine-linked frameworks could restrict the conductivity of the electrocatalytic system [107]. Therefore, additional conductive additives [37] or redox-active moieties [108] to enhance the catalytic performance are essential. Subsequently, the β-ketoenamine-linked COFs prepared via Michael addition-elimination reaction [109] have been reported. Over the next years, urea-linked COFs [110] were developed, showing the stability against boiling water and strong acid while the sensitivity to basic aqueous solutions. Analogically, the formation of COFs based on benzoxazole [111], benzothiazole [111], benzimidazole [112], phenazine [113], and pyrimidazole [114] relied on the reversible-irreversible reaction pairs of imine-cyclization, leading to the excellent chemical stability and the expansion of in-plane π conjugation. In 2014, polyimide COFs were designed and achieved, which are featured with abundant redox-active diimide carbonyl centers and the prominent chemical stability [115]. In 2017, in the presence of the strong electron withdrawing cyano groups, the report of highly stable and fully conjugated sp^2 COF appeared [116]. Thereafter, the unsubstituted sp^2 COF was obtained through the aldol condensation reaction [117]. Also in 2017, the devitrification from the amorphous polymers into the covalent amide frameworks under the reversible conditions of high temperature and high pressure was demonstrated, which could only be converted from imine bonds previously [118]. In the same year, the covalent organic gel framework based on viologen was fabricated via the Zincke reaction, assuming the unique radical cationic nature and the conspicuous sign of stability [119]. Recently, COFs linked by the dioxin [120] and ester [121] were declared to be added into the ever expanding library.

Currently, COFs comprised of boroxine [122], amine [62], triazine [24, 25, 123–125], imine [126, 127], β-ketoenamine [37], phenazine [16, 128–130], squaraine [131], olefin [132], imide [133], 1,4-dioxin [134], and porphyrin [135] have been successfully applied for the catalysis of N_2 reduction reaction (NRR), CO_2RR, HER, OER, and ORR.

3.3 Increase of the crystallinity

Typically, the synthesis of crystalline 2D COFs relies on altering experimental parameters that affect the crystallinity (monomer concentration, solvents, solvent ratio, catalyst, temperature, and pressure, etc.) in parallel and screening by powder X-ray diffraction (PXRD). The crystallinity, porosity, and processability of COF are subject to the influence of solvents, but unfortunately, there are few systematic studies to elucidate the underlying mechanism. Different from the solubility requirements of the preparation of thin films, powder COF could grow in heterogeneous solutions. Most often, the solvents used in the synthesis of powder COF will be trial-and-error and modified according to the conditions offered in the reports of the COF with similar structures.

3.3.1 Dynamic covalent chemistry

In the reactions accompanied by the reversible covalent bond generation, design principles derived from dynamic covalent chemistry are often used to increase the crystallinity of COF. DCC involves a series of reversible covalent chemical reactions based on thermodynamic equilibrium. Its reversible feature allows approaching the thermodynamic minimum of the system through proof-reading and error checking, which enables the exchange of

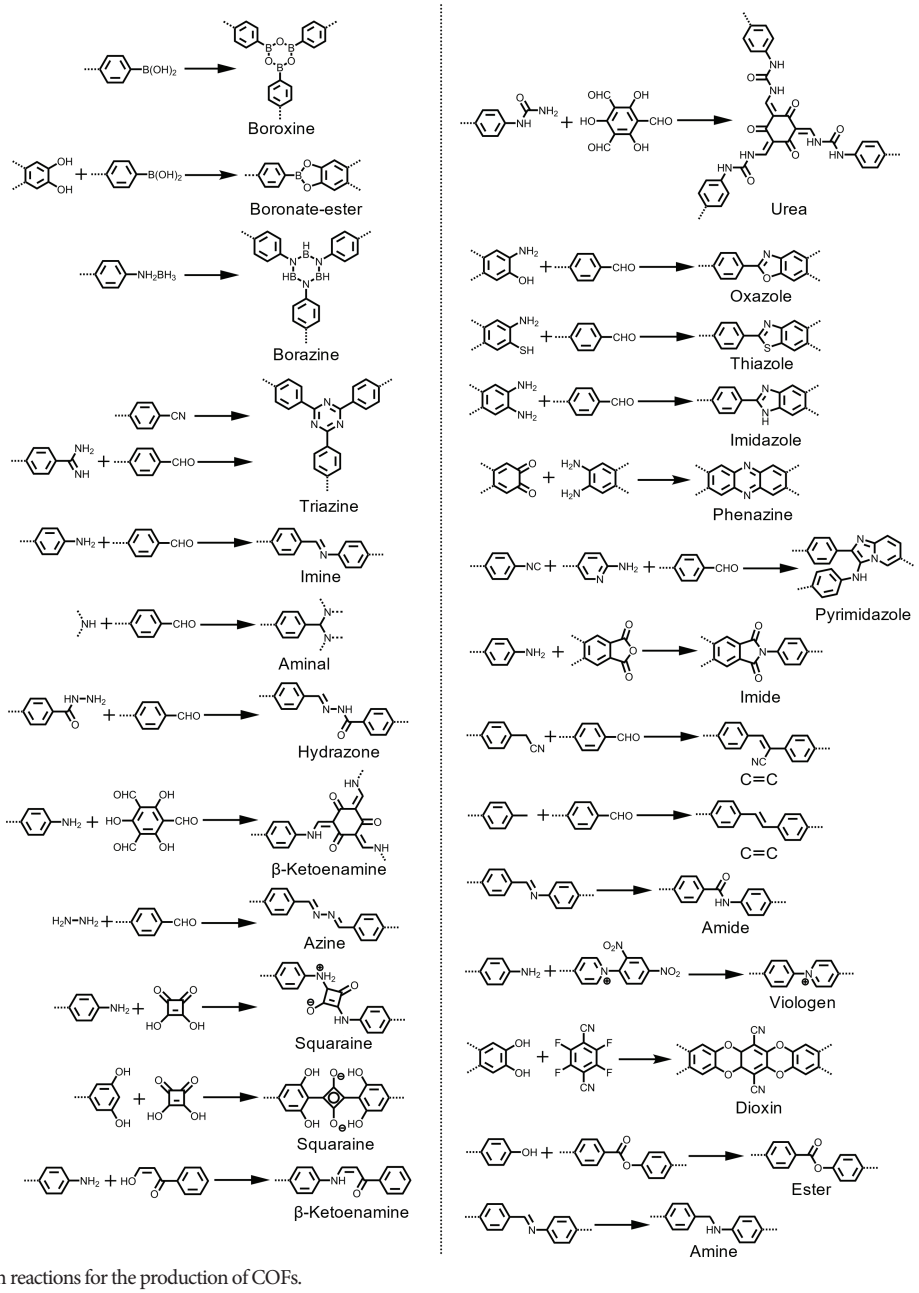

Figure 4 Polymerization reactions for the production of COFs.

building blocks. Currently, the transformations from covalent organic polymers (COPs) to COFs [28–30], linear polymers to COFs [136], COFs to COFs [137, 138], between COFs and cages [139] have been realized, which contain different linkers [29, 140, 141], different substituents [27, 30], and COF structures of different dimensions [142], and it has been designed for the construction of complex structure COFs [138], material functionalization [27], crystallization, and surface area enhancement [28–30, 137, 140, 141, 143]. It is worth noting that, based on the DCC as the main driving force, not all materials can be facilely accessible [29, 30, 136, 139, 142]. Thermodynamically stable products or functional groups with favored energy interactions are the decisive factors, and varying experimental parameters [27, 137, 138, 141] play a vital role in guaranteeing the crystallinity.

In the formation processes of borate and imine-linked COFs, adding water can maintain the reversibility for high-quality products. Smith et al. [86] studied the 1,3,5-tris(4-aminophenyl)benzene (TAPB)-terephthalaldehyde (PDA) COF system and detected that there was no precipitation with the lack of catalyst acetic acid, whereas the absence of water led to rapid precipitation of amorphous substances. Only the lowest concentration > 3.3 M H_2O and ≥ 1 M HAc can induce crystallinity and maintain high yields (Fig. 5(a)). Smith et al. [78] pointed out in the earliest study of the reaction mechanism of COF-5 that adding 15 equivalents of H_2O (relative to 2,3,6,7,10,11-hexahydroxytriphenylene (HHTP)) can afford the average crystal domain diameter of 40 nm, which is 4 times larger than that without H_2O (Fig. 5(b)). Wang and colleagues [144] introduced a small amount of $CuSO_4{\cdot}5H_2O$ into the closed reaction system as a water "reservoir" to regulate the chemical equilibrium of the dehydration reaction, thereby obtaining the highly ordered COF network on the surface of highly oriented pyrolytic graphite (HOPG). Moreover, under the condition of high temperature and high pressure, by the action of water, the reversible formation of amide bond was accessed, and the crystalline order was generated in the covalent amide framework [145].

In the case of imine-based COFs, besides the typical organic solvents and acetic acid catalyst, more emerging reagents and high-efficiency catalysts are encouraging. Tan et al. [148] encapsulated Fe_2O_3 nanoclusters by a disordered polyimine network. As a consequence of acid non-resistance of Fe_2O_3 core, pyrrolidine

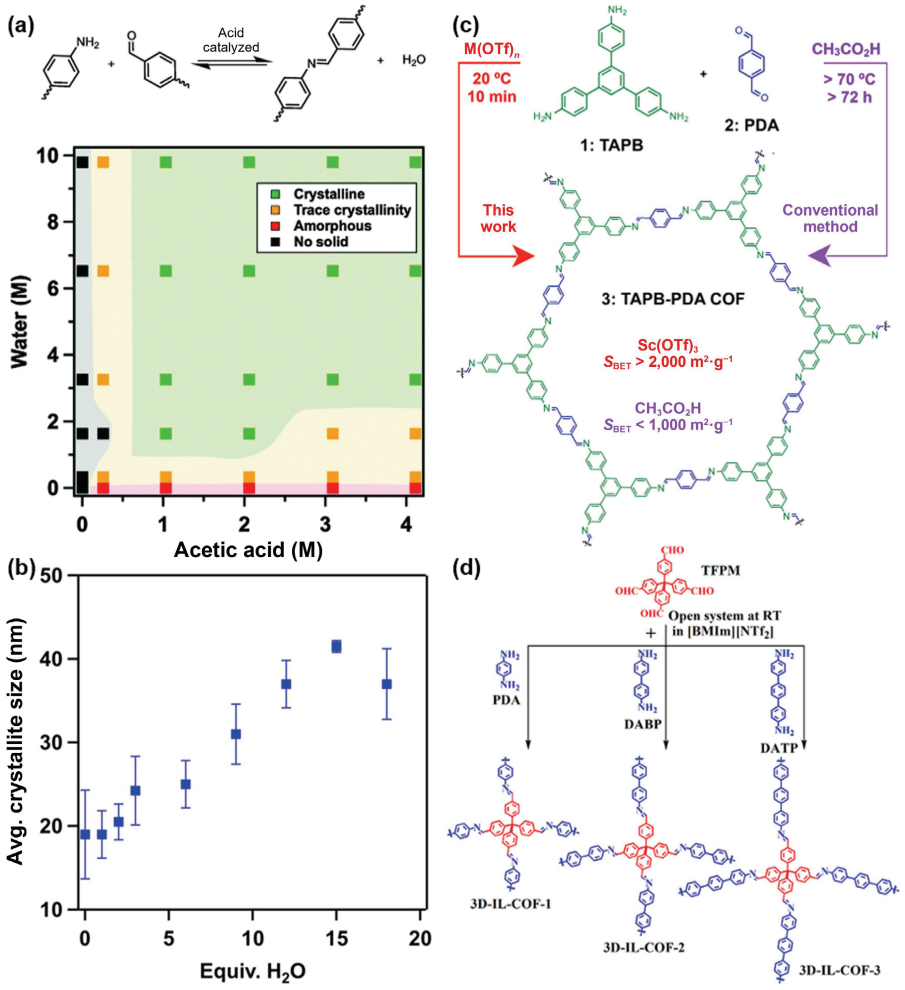

Figure 5 (a) COF synthesis as a function of acetic acid and water concentration. Reproduced with permission from Ref. [86], © The Royal Society of Chemistry 2016. (b) Crystallite size as a function of water equivalents. Reproduced with permission from Ref. [78], © American Chemical Society 2014. (c) Comparison of conventional catalyst and newly developed Lewis acid-catalyst to catalyzing the formation of TAPB-PDA COF. Reproduced with permission from Ref. [146], © American Chemical Society 2017. (d) Synthetic scheme for the 3D COFs in ionic liquids. Reproduced with permission from Ref. [147], © American Chemical Society 2018.

catalyzes the recrystallization from amorphous polymer to imine-linked COF, and greatly elevates the Brunauer–Emmett–Teller (BET) surface area of bulk COF to 1,883 $m^2 \cdot g^{-1}$. Karak et al. [149] chose a series of Bronsted acids as catalysts and modulators to form acid-diamine salts with diamine monomers. This protonation–deprotonation of acid and diamine is a reversible reaction, which competes with the imidization reaction to lower the reaction rate, maintain the reversibility of the reaction, and promote the formation of highly crystalline and porous COF. Nonetheless, strong hydrogen bonds will obstruct the formation of imine bonds, and weak hydrogen bonds lead to less ordered structures. Therefore, it is observed that the hydrogen bond distance $d_{avg}(N_{amine}–H\cdots O_{acid})$ in the acid-diamine salt is 2.06–2.19 Å, and COF presents a similar high surface area and crystallinity. Dichtel and his colleagues [146] suggested that under the catalysis of metal triflate, only 10 min at room temperature, the synthesis of imine-linked COF with BET surface area as high as 2,175 $m^2 \cdot g^{-1}$ pays for, which is much higher than the previous solvothermal conditions (Fig. 5(c)). The same catalyst was applied for the synthesis of COF films at the liquid–liquid interface, affording large-area, continuous COF films with thickness ranging from 2.5 nm to 100 μm [150]. Unfortunately, only thick films were crystalline with the absence of sharp diffraction peaks. This demonstrates that the transition between high-quality powder isolated from the solution and the crystalline films polymerized at the interface requires some special design and optimization for the ordered arrangement of COF films.

In recent years, ionic liquids with physicochemical properties tunable by the counter anions have been developed as a medium to synthesize imine-linked 3D COF within 12 h under milder conditions than solvothermal method, and even the synthesis of 3D COF with specific structure only takes 3 min (Fig. 5(d)) [147]. Jiang et al. [151] achieved the synthesis of 2D TFPPy-PDA-COF and TFPPy-PyTTA-COF in ionic liquids, and tried ionic liquids with different counter anions as solvents. Only 1-butyl-3-methylimidazolium bis((trifluoromethyl)sulfonyl)imide ([bmim][NTf_2]) provided high-quality microcrystals, that may originate from the trigger of the interaction between π and the ionic liquid cations and the arrangement of aromatic units into ordered structures [152]. Wang et al. [153] synthesized the highly crystalline hierarchically porous COFs in the presence of catalytic amounts of 1-alkyl-3-methylimidazolium tetrafluoroborates ([C_4mim][BF_4]), but only amorphous polymers in the neat dimethyl sulfoxide (DMSO). Interestingly, the mesopores in IL-mediated samples were not found in traditional COF, whose size and proportion were tuned by varying the alkyl chain length of the ionic liquids. Azine [154], imide [155], and β-enamine-linked COFs [155, 156] and COF membranes [157] were continuously obtained via the ionic liquids.

Monofunctionalized molecules are regarded as modulators (Fig. 6), and added in the synthesis system, to compete with the multifunctional bridging monomers, slow down the nucleation processes [78, 158, 159], adjust the growth direction [159], control the shape and size [160–162], and even realize the

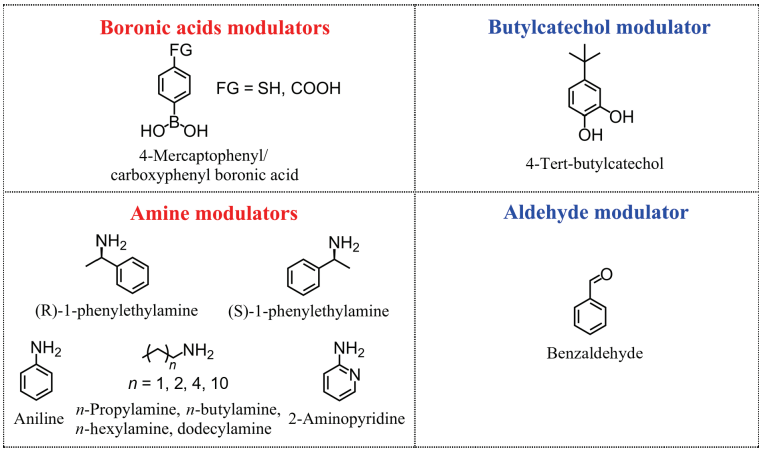

Figure 6 Monofunctionalized molecules added in the synthesis of 2D COFs.

functionalization of materials [158]. Bein et al. [158] demonstrated the enhancement of the crystallinity, BET surface area, and pore volume in the presence of small quantities of monodentate boronic acids with thiol and carboxylic acid groups as modulators, and the functionalization of the COF grain boundary edge. Dichtel et al. [159] inhibited the precipitation of COF powder by adding the competing 4-tert-butylcatechol. Further kinetic investigation proved that mono-catechol species effectively retarded the occurrence of nucleation, decelerated the relative rate of in-plane and out-of-plane growth, and improved the crystallinity of preformed particles. The same improvements of the crystallinity and morphology-controlled synthesis initiated by modulators have also been shown in the generation of imine COFs. In addition, the chiral modulators (R)- or (S)-1-phenylethylamine induce achiral precursors to crystallize the chiral COFs [52]. 3D COF single crystals COF-300, COF-303, LZU-79, and LZU-111 suitable for single crystal X-ray diffraction (SXRD) analysis were grown by the modulation of different optimal concentrations of aniline [163]. And the size of single crystals can be rationally tuned by adjusting the aniline concentrations. As the follow-up, the non-interpenetrating single crystal LZU-306 was synthesized with the same modulator [164]. Esteves et al. [165] evaluated the COFs named RIO-11, RIO-12, and RIO-13, obtained by the condensation of aldehyde monomers with different numbers of hydroxyl groups and hydrazine hydrate, and found that RIO-11 who owns one hydroxyl group showed the lowest crystallinity and surface area, while the improvement in material properties gradually flattened out with the increase in the number of hydroxyl groups. Using aniline as the modulator, RIO-11 lacking conformational lock can benefit from the modulating method, but it is not suitable for improving the crystallinity of RIO-12 and RIO-13 with more intramolecular hydrogen bonds. Apart from aniline, benzaldehyde as the competitor of the condensation of TAPB and PDA or 1,3,5-tris(4-formylphenyl)benzene (TFPB), the sharpening (100) diffraction peaks and the increases in BET surface area were observed [166]. Furthermore, the combination of benzaldehyde and aniline was employed in the polymerization of TAPB and 1,3,5-benzenetricarbaldehyde (BTCA) catalyzed by $Sc(OTf)_3$, providing the COF with the higher crystallinity and the double surface area than that without competitors, and the quality of materials was improved even further when the increased amount of acid catalyst was added [161]. Evidenced by the relative ratio of the PXRD peak, the addition of 12 equivalent of modulators provided the largest crystallites, and the further increase of the equivalent ratio of modulators led to the significant decrease in sample yield. COF products can be reconstructed through the "reversible polycondensation termination" (RPT) process even after the formation, and components with less-crystallinity were selectively removed. This phenomenon did not occur with the addition of only one modulator. Liu et al. [167] attempted monofunctional monomers such as *n*-propylamine, *n*-butylamine, *n*-hexylamine, *n*-dodecylamine, and 2-aminopyridine, which not only shortened the polymerization time under ambient pressure, but also afforded the better-crystalline COFs.

3.3.2 *Pre-assembly of building blocks*

Pre-assembly aligns the building blocks via the external force or weak interaction to promote the orderly arrangement of monomers, and then the polycondensation transforms the weak interaction into a stronger covalent bond and connects the building blocks. The method is similar to the surfactant-monolayer-assisted interfacial synthesis (SMAIS) developed by Feng and colleagues. The monolayer of the anionic surfactant sodium oleyl sulfate (SOS) on the water surface, in virtue of the electrostatic interaction and hydrogen bonding between SOS and the protonated porphyrin or triazine, directs the pre-assembly of the monomer and facilitates the polymerization in the confined space between surfactant and water surface. The monomer is vertically anchored under the monolayer of surfactant octadecanoic acid (SA) through the covalent amide bond, tuning the growth direction from horizontal to vertical. The general and efficient synthesis of few-layer polyimide films (about 2 nm thickness, average crystal domain size of 3.5 μm^2) [168], multilayer polyimine films (thickness ranging from 6 to 200 nm, domain sizes of 100–150 nm) [169], and boronate ester COF films (tunable thickness from 6 to 16 nm, maximum crystal domain up to ~ 60 μm^2) [170] were demonstrated.

3.3.3 *Driving force control of polycondensation*

In order to control the driving force of polycondensation and support self-repair of crystal defects, the most obvious way is the slow supply of monomers. As mentioned in the first COF paper [67], the solvent affected the solubility of the monomer and controlled the diffusion of the linkers. Equally, the ventilation-vial protocol was proposed for the low-temperature production of 3D COF-300 crystals, in which the volatilization of dioxane reduced the solubility of the components and generated the acidity gradient, helping to control the homogeneous nucleation of the crystals [171]. Hao et al. [172] loaded the two monomers into oil and hydrogel respectively and formed the superspreading thin liquid layer by water on the surface of the hydrogel, providing the oil/water/hydrogel interface for the polymerization of oriented COF films. The diffusion of the monomer from hydrogel to water takes 1 h to reach equilibrium, thus the ability to slowly release the monomer promotes the growth of crystalline COF. Similarly, through decline of the reactant concentration to be nucleated

directly, stable and well-dispersed COF nanospheres with high crystallinity and porosity were synthesized in dichloromethane [173]. Subsequently, the liquid–liquid interface between water containing a catalytic amount of trifluoroacetic acid and COF dispersed solution was constructed, at which the nanospheres spontaneously assembled and fused, and the COF film with increased crystallinity and porosity compared to NPs was prepared. It is the first report to demonstrate the mesoscale covalent self-assembly from uniform COF colloidal solution based on a reversible reaction to the continuous defect-free thin film at the liquid–liquid interface. It is wise for the artificially slow addition of building blocks, which has proven to be beneficial for the synthesis of highly crystalline CTFs [174], and the growth of COF NPs [175] even large single crystals [176].

Designing precursors to regulate the *in-situ* formation of linkers is also the elegant way for crystallinity enhancements (Fig. 7). Similar to the mechanism of the modulated methodology in two steps [165], the imine precursors also spark off the transimination. N-arylbenzophenone imine can be substituted for amine monomers in the synthesis of imine and β-ketoamine linked COFs, and its slow deprotection gives rise to the adjustable free amine functionality and the enhanced material quality [177]. Likewise, a series of COFs were constructed via Michael addition elimination reaction at ambient temperature and pressure using β-ketoenamine replacing β-ketoenol, and synthetic times were cut down to less than 8 h [178]. The tert-butoxycarbonyl protected amine has been found to afford the high-quality COF crystals [179]. The amine monomers were deprotected *in-situ* with trifluoroacetic acid to advance the homogeneous growth and prevent the generation of amorphous intermediate precipitates, thereby giving the high-quality crystalline imine-linked woven COF, nanocrystals, and films. Tan et al. [93] demonstrated the utility of the slow oxidation of alcohols to the aldehyde monomers by crystallizing the CTFs, most of which were amorphous and carbonized. It should also be noted the precise temperature control. The initial low temperatures caused the concentration of crystal nuclei, and the subsequent high temperatures profited the faster crystal growth. Acetals have been reported as alternatives to aldehydes, possessing better stability and solubility [180]. Boronate ester-linked COFs have also been constructed from protected monomers, such as the acetonide catechol [181, 182] and the dioxaborolane [183]. Because of the high reversibility of this polycondensation, the differences in the surface area and crystallinity when comparing the boronate ester-linked COFs are not as prominent as that of other linked COFs, so the addition of protecting groups are aimed at better solubility and the oxidation resistance.

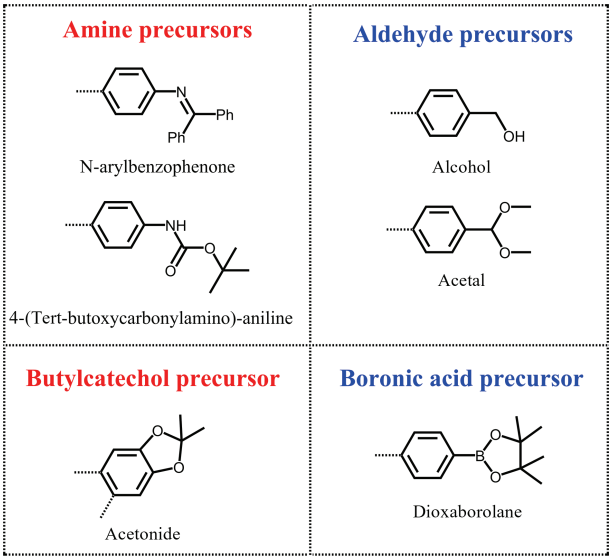

Figure 7 Precursors used in the synthesis of 2D COFs.

3.4 Ultra-thinning

COF powder is often made into ink together with chemical binder nafion and conductive carbon material, and it is drip-cast onto the electrode surface for catalysis. However, it leads to nonuniform COF deposition, which not only increases the interface resistance and limits the diffusion of electrons, but has access to a handful of catalytic sites [126]. Thus, controlling thickness of the layer has broad scientific and technological significance in the field of electrocatalysis.

In theory, the specific surface area of few-layer films higher than that of multi-layer films and more accessible active sites in ultrathin nanosheets could result in the superior electrocatalytic performances. Zhu et al. [184] designed a range of metalloporphyrin-tetrathiafulvalene based COFs (M-TTCOFs), and the FE_{CO} value of Co-TTCOF after exfoliation was higher than 90% in a wide potential range of −0.6 to −0.9 V and the maximum FE_{CO} can reach up to 99.7%, which is higher than unexfoliated one and the highest among reported COF at that time. Therefore, nanosheets are considered as ideal materials for electrocatalysis.

The fabrication of covalent organic nanosheets (CONs) is classified into the top-down method by peeling off nanosheets from bulk materials prepared by standard COF synthetic procedures, and the bottom-up method in which nanosheets are grown from monomers.

In layered COFs, due to the strong covalent bond in the plane and the weak π–π stacking force out of the plane, it is feasible to exfoliate the 2D COF by internal or external forces. Ultrasound is a common external mechanical force to break the non-covalent interactions between COF layers, and optimizing the experimental parameters such as temperature, power, and time, ensures the achievement of large lateral dimensions under the premise of single- or few-layered sheets. Additionally, choosing appropriate solvents or efficient intercalators to expand the interlayer distances and weaken the interactions is also the pivot of the effective exfoliation.

Inspired by the successful exfoliation of graphene through ultrasonic treatment, in 2011, Berlanga et al. [185] first reported the sonication for COF nanosheets. 10–25 layers of CONs were exfoliated from the COF-8 powder in anhydrous dichloromethane, present in the supernatant after centrifugation. In further research, a series of C–C coupled rigid microporous poly(aryleneethynylene) networks with pores of diameter from 1.4 to 3.3 nm were used to explore the influence of porosity and processing time on the degree of exfoliation [186]. The results revealed that smaller pore sizes and longer sonication time caused thinner CONs. Unfortunately, even in the best case, the separated nanostructures still consisted of 5–6 stacked layers, rather than the monoatomic layer. The nanosheets with the thickness of 0.5 nm corresponded to a single layer were also successfully transformed from the pristine COF-1 through the sonication treatment in dichloromethane, which were coated on the outside surface of macroporous α-Al_2O_3 support to assemble a smooth and continuous COF film [187]. Compared with the borate ester based COF-1 and COF-8, the hydrazone-linked COF with better chemical stability and lack of interlayer B–O Lewis acid-base interactions, is facilely exfoliated to 2D COF nanosheets under the less solvent restriction. Dichtel and colleagues [188] investigated the relationship between solvents and the exfoliation yield, because they found the crystallinity loss of COF-43 in dioxane, H_2O, and DMF, which is different from other solvents (such as tetrahydrofuran (THF), $CHCl_3$, and MeOH). Atomic force

microscopy (AFM) suggested polymers deposited from dioxane with lateral widths of 200 nm and average heights of 1.32 nm (corresponding to 3–5 layers), and dispersions in water as thin as 3.3 Å, while in non-exfoliating solvents were much thicker, even aggregate in MeOH. Osakada and colleagues [189] carried out the Schiff-base condensation reaction between 5,10,15,20-tetrakis(4-aminophenyl)-21H,23H-porphyrin (Tph) and dihydroxyterephthalaldehyde (Dha) to prepare the COF (DhaTph) with unique photochemical properties as a catalyst for photocatalysis HER, and realized the exfoliation of porphyrin-comprised COFs in five common solvents: dichloromethane, methanol, pyridine, nitrobenzene, and water. The exfoliation occurs effectively when the surface energies of materials and solvents are close. They revealed that thinner nanodisks could be exfoliated by increasing the reaction temperature and time, turning the surface energy of the solvent, and applying mechanical force through stirring. This sonication strategy can also be assisted by other solvents, such as isopropanol [190], chloroform [191], water [192], and toluene [109].

The exfoliation strategy is not merely limited to solvents as intercalating molecules, but also employs the intercalating agents. Zhao et al. [193] applied the temperature-swing gas exfoliation approach (Fig. 8(a)) for the first time to the fabrication of nanosheets with the thickness of about 2–4 nm. They employed 1,1,2,2-tetrakis(4-formyl-(1,1'-biphenyl))ethane (TFBE) as the monomer for the targeted synthesis of three imine-based and azine-based 2D COFs called NUS 30–32. The bulk materials of NUS 30–32 were heated in the air at 300 °C for 10 min, and then immediately immersed in liquid nitrogen until the liquid nitrogen vaporized completely. In this process, the high temperature increases the interlayer space, and the subsequent gasification of liquid nitrogen exfoliates the COF powders effectively. Chen et al. [194] inserted *in-situ* growth MnO_2 NPs via the reaction of $KMnO_4$ and $HClO_4$ into TFPB-COF (Fig. 8(b)), which was subjected to sonication and transformed to platelets with thickness of 1.6 nm, and then removed MnO_2 with hydrochloric acid. In the same way, *n*-butyl lithium (*n*-BuLi) functions as intercalator to exfoliate the COF composed of TFP and PDA [195]. According to the *trans*- to *cis*-isomer transition of azobenzene under ultraviolet light, Yao et al. [196] developed azobenzene-assisted exfoliation method and systematically studied influencing factors for efficient exfoliation, including the amount of azo, matching of the COFs structure, and ultraviolet (UV) irradiation time, etc. The azobenzene content above 50% led to the improved exfoliation, while too much doping partially blocked the channels inside the COF and affected the surface area and crystallinity. And the monomers whose C_2 symmetrical structure is similar to azo, larger-scale CONs can be easily prepared. All of the above, and based on

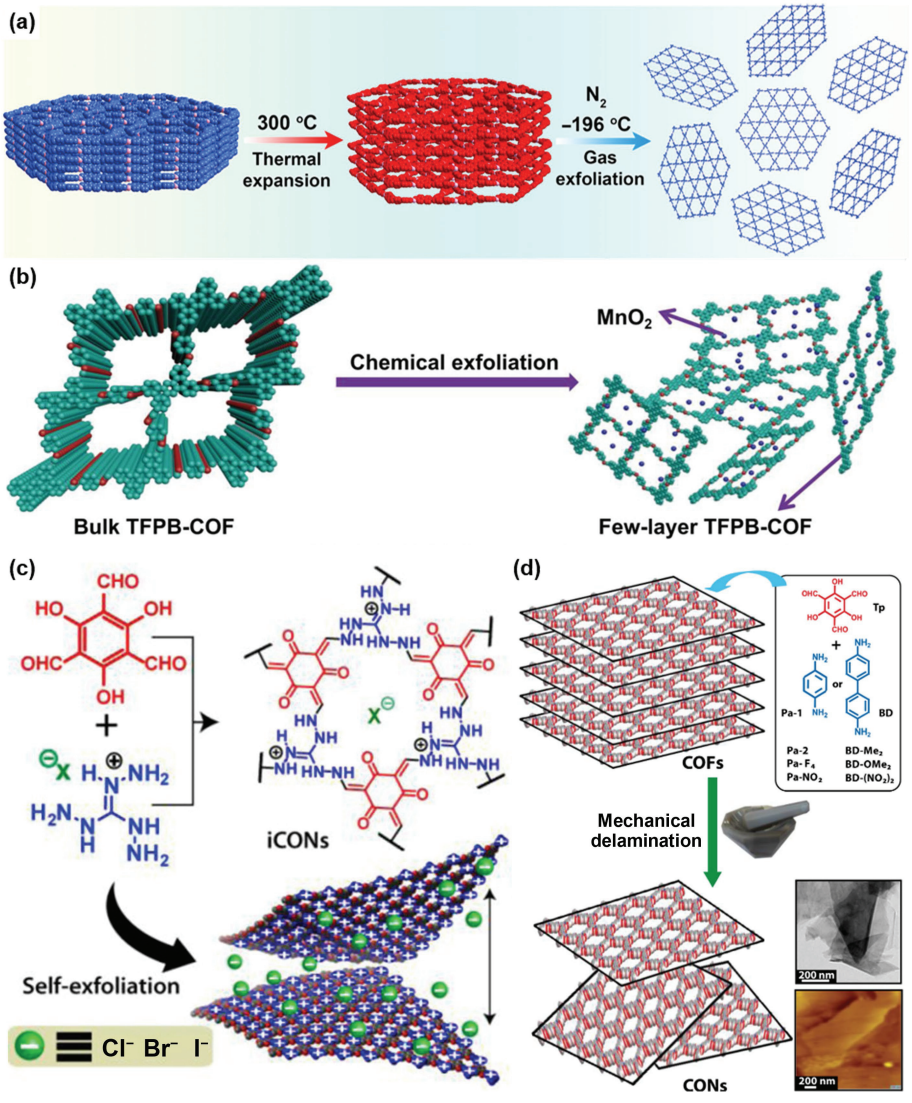

Figure 8 (a) Schematic illustration of the temperature-swing gas exfoliation. Reproduced with permission from Ref. [193], © American Chemical Society 2018. (b) Schematic illustration of the chemical exfoliation with MnO_2 NPs as intercalator. Reproduced with permission from Ref. [194], © WILEY-VCH Verlag GmbH & Co. KGaA, Weinheim 2019. (c) Schematic representation of the synthesis of iCONs and exfoliation. Reproduced with permission from Ref. [197], © American Chemical Society 2016. (d) Schematic illustration of the preparation of CONs. Reproduced with permission from Ref. [198], © American Chemical Society 2013.

the difference in the irradiation time required for the conversion of azo and azo structural units in COFs, as well as the effect of sonication time on the size of nanosheets, large-area and few-layer nanosheets with size up to 4.0 μm × 2.5 μm and thickness of only 1.8 nm were produced when introducing 50% azobenzene, measuring UV radiation for 12 min, and conducting ultrasonic treatment for 0.5 min.

Conversely, the self-exfoliation strategy exploits the chemical design and introduces the repulsive electrostatic forces or non-planar building blocks into COF skeletons to break the interlayer stacking interactions and assist the exfoliation of layered materials. Encoding the high charge density into the framework hampers the inter-layer π–π stacking and provides COF colloid for excellent solubility, resulting in solution-processable yet crystalline 15 nm thick PyVg-COF nanosheets [199]. The imine-linked COF can be protonated by acid treatment and exfoliated into nanosheets [200]. Banerjee et al. [197] introduced the positively charged guanidinium units into the COF structure, causing interlayer repulsion to self-exfoliate into ionic CONs (iCONs) with height profile of 2–5 nm (Fig. 8(c)). Bai et al. [201] designed anthracene-based ionic COFs (iCOFs-A) as well as non-ionic COFs (COFs-B), and investigated the effect of different polar organic solvents on the stripping of iCOFs-A. Due to solvation, iCOFs-A exhibited multiple layers, sheets curled into balls and platelets with the average diameter of 20 μm and thickness of 3.5 nm in dioxane/mesitylene (1/1), dioxane and acetonitrile, respectively. The experience proved that electrostatic repulsion and high polarity solvents are indispensable for COF self-exfoliation. Ajayaghosh and colleagues brought ethidium bromide [202] or propidium iodide [203] to COF, and dispersed them in deionized water into cationic nanosheets. The competitive supramolecular host–guest interactions between cucurbit[7]uril (CB[7]) and 1-adamantyl-amine hydrochloride (AD), with quaternary ammonium groups, were exploited to reversibly control the multiple exfoliation and re-stacking of the iCONs.

Opposite to iCONs, non-ionic CONs have large branches or joints to generate steric repulsion or form a non-coplanar structure, which can withstand the interlayer π–π stacking. For instance, choosing flexible molecules with C_{3v} molecular symmetry [204], or triazole moieties [205, 206] as building units, increases bone flexibility and achieves the self-exfoliation. In addition, taking advantage of the [4 + 2] cycloaddition reaction between maleimide [207] or maleic anhydride [208], anthracening to distort the planarity of the anthracene-based COF skeleton, and increasing the steric hindrance between layers, CONs can be prepared without ultrasonic treatment.

Mechanical exfoliation is an effective method to employ mechanical shearing force to disintegrate the interaction between layers for solid CONs. Benerjee et al. [198] applied the mechanical grinding to eight chemically stable bulk COFs of the TpPa and TpBD series (Fig. 8(d)). Nanosheets with thickness range from 3 to 10 nm were synthesized by adding 1–2 drops of methanol to a mortar and grinding for 30 min at room temperature. Fourier transform infrared (FT-IR) and Raman spectroscopies of CONs showed the completely similar spectra like the parent COFs, indicating that the compositions and bonding mode were still intact after mechanical grinding. Wang et al. [209] delaminated the anthraquinone-based COF at room temperature through ball milling without additional exfoliating agents for CONs with almost 5 nm thickness.

The bottom-up approach is accustomed to converting small molecules directly into nanosheets in one step, whose mechanism responsible for ultra-thin CONs depends on the well-designed ionic building blocks and the increasing curvature of the skeleton, similar to the self-exfoliation. Zhao and colleagues [210] prepared two iCONs with ethidium and sulfonate groups via the gas–liquid interface synthesis strategy, namely cationic TpEBr and anionic TpPa-SO_3Na nanosheets (Fig. 9(a)). The thicknesses of TpEBr and TpPa-SO_3Na were 3 and 2.5 nm, respectively (Fig. 9(b)). Subsequently, the oppositely charged iCONs were horizontally transferred to the porous α-Al_2O_3 support layer by layer (LbL) by the Langmuir–Schaefer (LS) method. Driven by electrostatic attraction (Fig. 9(c)), iCONs assembled into ultra-thin films with a thickness of tens of nanometers (Fig. 9(d)), the membranes with controllable thickness, reduced aperture size, compact, and staggered stacking, are appropriate for molecular sieving gas separation. Jiang et al. [211] fabricated a series of COF nanosheets with a thickness of 1–2 nm by adding excessive 2,4,6-trimethylbenzaldehyde (TBA) under solvothermal conditions (Figs. 9(e) and 9(f)). Abundant TBA molecules allow the primary occupation of the edges for the initial oligomers and CONs, and are almost perpendicular to the surface of the COF, thus leading to anisotropic growth along the planar direction and limiting the further aggregation of thin layers. In addition, the LB strategy enables the production of the CONs to possess larger lateral size and higher aspect ratio [212]. Numerous examples of the LB method can be found in Section 3.2.

4 2D COFs for electrocatalysis

Among diverse methods for energy conversion, electrocatalysis reactions have been recognized as one of the most direct and effective pathways to achieve the interconversion between electrical energy and chemical energy. Electrocatalysis technique mainly depends on catalysts to accelerate the charge transfer on the interface of electrode and electrolyte, which plays a vital role in sustainable energy for carbon cycle [213]. In order to obtain favorable electrocatalysts with excellent catalytic activity, selectivity, and durability [214], tremendous effort has been devoted to modifying COFs as high-performance electrocatalysts by virtue of numerous advantages below: (1) The covalent bonds in COFs provide a high chemical and thermal stability. (2) The porous structure of COFs can expose more active sites in the electrolyte. (3) The periodic and regular structure of COFs is in favor of precisely controlling the active sites and pore size. (4) COFs can be used as precursors to synthesize porous and functional heteroatom-doping carbon-based materials

In comparison with 3D COFs, 2D COFs possess a relatively faster electron transfer rate and better electroactivity due to their π-stacking between layers [182]. Therefore, more attention is paid to the electrocatalytic applications of 2D COFs and some crucial strategies have been proposed to effectively promote intrinsic electrocatalytic activity. Actually, there still remain some shortcomings that severely impede the large-scale applications of 2D COFs in electrocatalysis such as poor electron-transfer capability. Thus, in this section, 2D COFs-based nanomaterials applied in various electrocatalytic fields (CO_2RR, HER, OER, ORR, and NRR) were systematically introduced here and the typical modification strategies to optimize COFs-based electrocatalysts were also summarized systematically.

4.1 CO_2RR

Nowadays, the massive emission of greenhouse-gas has become an urgent problem of human survival. The reasonable treatment of CO_2 as the main greenhouse gas is the orientation of the collective efforts of scientists. CO_2RR as one of ideal CO_2 fixation strategies aimed at converting CO_2 into value-added fuels or other chemicals (such as carbonic oxide and methyl alcohol), and it plays a crucial role in carbon cycle process. To elevate the efficiency of carbon cycle, a large current density, good selectivity,

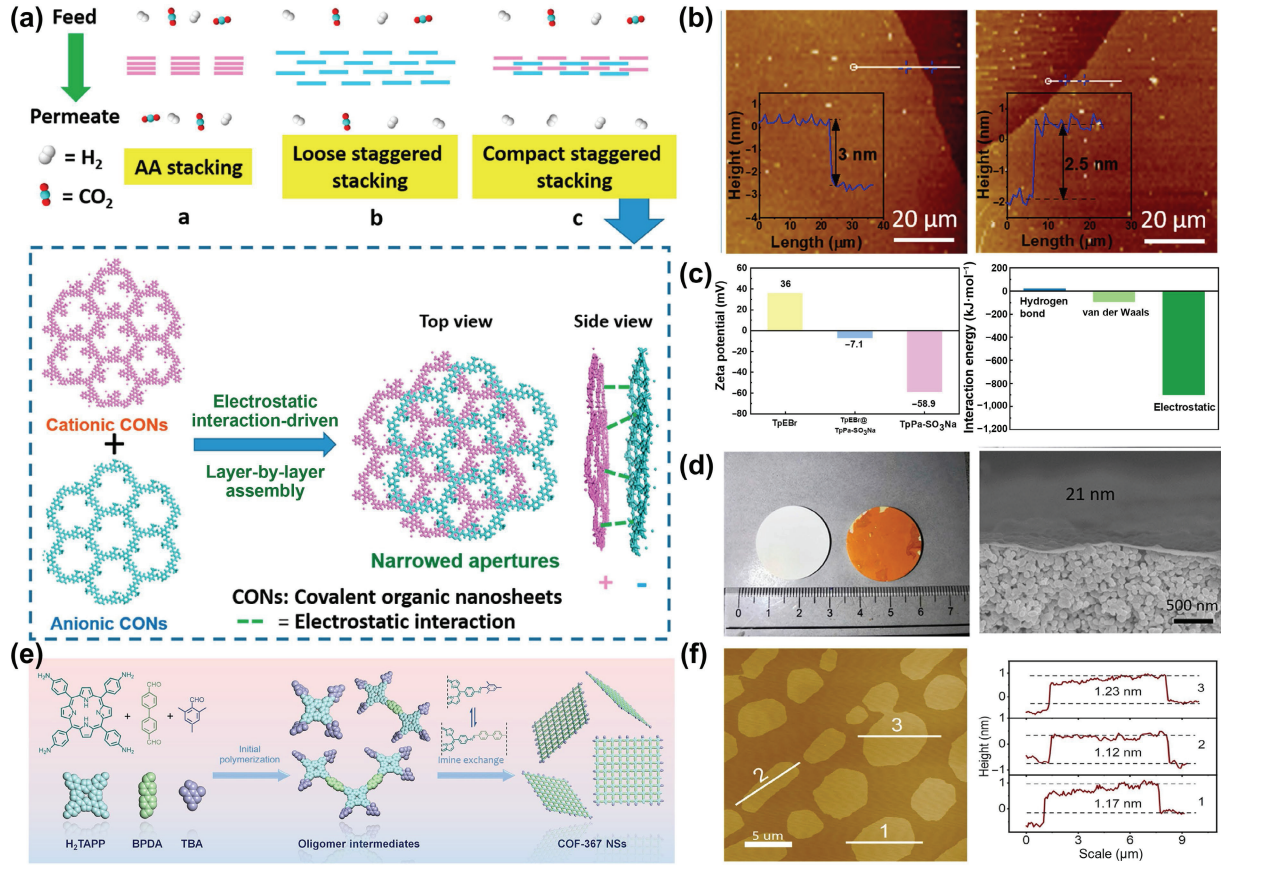

Figure 9 (a) Schematic illustration for LbL assembly of cationic TpEBr, anionic TpPa-SO_3Na nanosheets, and the membranes for gas separation. (b) AFM images of cationic TpEBr (left) and anionic TpPa-SO_3Na (right) nanosheets. (c) Surface zeta potentials (left) and molecular dynamics (MD) simulations (right). (d) Digital image of the comparison of the bare support with the membrane (left) and cross-sectional scanning electron microscope (SEM) image of the membranes (right). Reproduced with permission from Ref. [210], © American Chemical Society 2020. (e) Synthetic scheme of the COF-367 nanosheets (NSs). (f) AFM image and the height profiles along the white line of COF-367 NSs. Reproduced with permission from Ref. [211], © American Chemical Society 2019.

long-time durability, and superb energy efficiency for CO_2RR electrocatalysts are the major development goals [215].

To address the problem of inherently poor electron-transfer capability for COFs, Wu et al. [216] integrated tetrathiafulvalene (TTF), which served as an excellent electron relay mediator, into as-synthesized 2D cobalt porphyrin-based COF (Fig. 10(a)). The conductivity measurements by the powder pellet two-electrode method showed that the electron conduction of TTF-Por(Co)-COF (1.32×10^{-7} S·m^{-1}) was higher than COF-366-Co (6.5×10^{-9} S·m^{-1}). Enhanced electrical conductivity was attributed to efficient electron transfer from the TTF to the cobalt porphyrin ring in TTF-Por(Co)-COF. The DFT calculations revealed that TTF-Por(Co)-COF had a lower barrier than COF-366-Co in the CO_2RR process. To evaluate the selectivity of catalysts, reduction products were analyzed at different potentials by gas chromatography (GC) and nuclear magnetic resonance (NMR), and the results showed CO_2 was reduced to CO without liquid product. Compared with COF-366-Co (FE: 70.8%) in Fig. 10(b), TTF-Por(Co)-COF achieved a higher activity for conversion of CO_2 to CO with high FE of 95% at −0.7 V vs. RHE. At −0.7 V vs. RHE in CO_2-saturated 0.5 M $KHCO_3$, TTF-Por(Co)-COF owned the acceptable stability even if the current density decreased 50% (Fig. 10(c)). This study demonstrated that the introduction of electron transporter into COFs was an effective way to improve the electron transport rate and the capability of CO_2RR.

On the basis of the analogous strategy, Zhu et al. [184] chose TTF as the electron donator or carrier in as-obtained metalloporphyrin-tetrathiafulvalene based COFs (M-TTCOFs) and the CO_2RR performances of a series of M-TTCOFs (M = Co or Ni) were compared (Fig. 10(d)). As Fig. 10(e) shown, a highly ordered porous structure can be observed by high-resolution transmission electron microscopy (HR-TEM). The N_2 and CO_2 sorption tests displayed that Ni and Co dopings can enhance the adsorption capacity. In Fig. 10(f), the smaller Tafel slope of Co-TTCOF (237 mV·dec^{-1}), compared with Ni-TTCOF (629 mV·dec^{-1}) and H_2-TTCOF (433 mV·dec^{-1}), demonstrated good kinetics of Co-TTCOF in conversion of CO_2 to CO. The partial CO current density of Co-TTCOF was 1.84 mA·cm^{-2} at −0.7 V, which was more than those of Ni-TTCOF (0.15 mA·cm^{-2}) and H_2-TTCOF (0.079 mA·cm^{-2}). The maximum FE_{CO} value (Fig. 10(g)) at −0.7 V of Co-TTCOF (91.3%) was higher than other M-TTCOFs (Ni-TTCOF, 20.9% and H_2-TTCOF, 4.22%). After the chronoamperometric test for 40 h, Co-TTCOF exhibited excellent CO_2RR stability with neglectable decay in activity, and the corresponding FE_{CO} can be retained at > 90%, which illustrated Co-TTCOF was a stable electrocatalyst. Based on the experiment results and theoretical calculations, they proposed possible mechanism and reduction processes of Co-TTCOF from CO_2 to CO. TTF, which played a role as a kind of electron sponge and donator in favor of high electron mobility, formed efficient electron transmission pathway with metalloporphyrin. During the electrocatalytic CO_2RR process, TTF initially obtained the electron from the electrode and efficiently transfered it to Co centers under the help of the electron transmission pathway.

Inspired by metal phthalocyanines as active sites for CO_2RR reported before [217, 218], Liu et al. [130] introduced nickel phthalocyanine into conductive pyrazine-linked conjugated 2D COF (NiPc-COF) for CO_2RR application (Fig. 11(a)). The electrical conductivity of as-prepared NiPc-COF reached 3.77×10^{-6} S·m^{-1} beyond those of insulating COFs [116]. By comparison

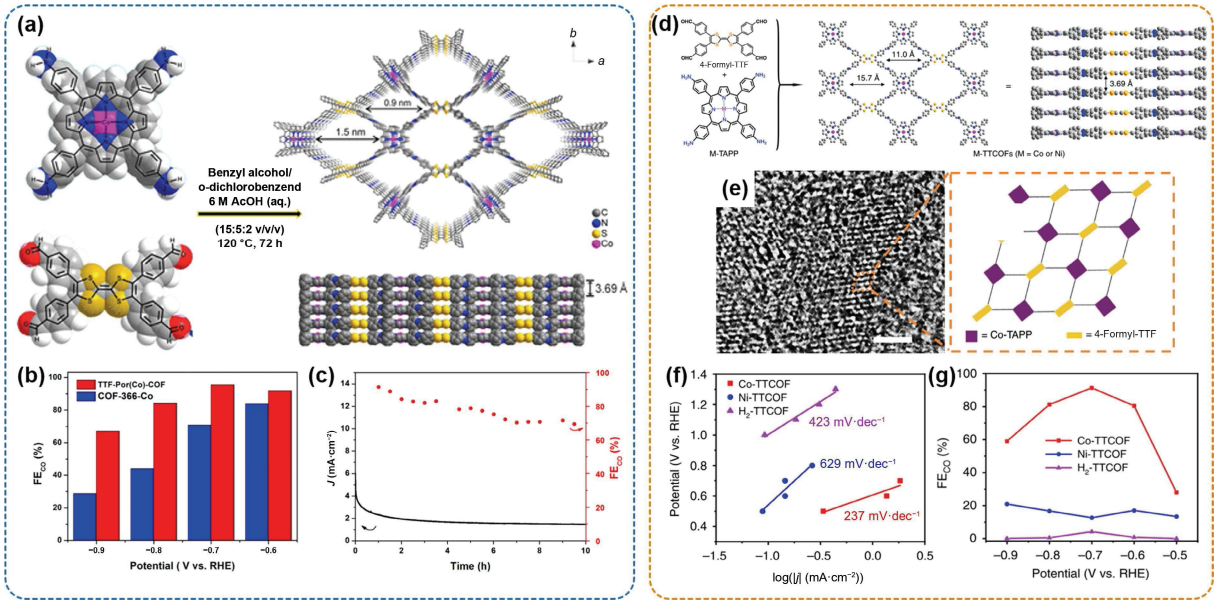

Figure 10 (a) Schematic illustration of the synthesis of 2D TTF-Por(Co)-COF. (b) FE_{CO} from −0.6 to −0.9 V of TTF-Por(Co)-COF and COF-366-Co. (c) The stability test of TTF-Por(Co)-COF. Reproduced with permission from Ref. [216], © American Chemical Society 2020. (d) The structure image of M-TTCOFs. (e) HR-TEM image (scale bar: 2 nm). (f) Tafel plots. (g) FE_{CO} from −0.9 to −0.5 V. Reproduced with permission from Ref.[184], © Zhu, H. J. et al. 2020.

with the LSV curves, the curves in CO_2-saturated electrolyte had a more positive onset potential (−0.55 V) and higher current densities, demonstrating high CO_2 reactivity for the NiPc-COF. Besides, the NiPc-COF nanosheets showed very a high CO selectivity with FE (Fig. 11(b)) over 93% in the wide applied potential range of −0.6 to −1.1 V and also achieved a largest CO partial current density of 35 mA·cm^{-2} at −1.1 V. In the aspect of the stability, a steady reduction current density was kept for 10 h and high FE was over 98% without downward trend. These experimental results demonstrated that the conjugated pyrazine units to the accessible nickel phthalocyanine active sites of NiPc-COF nanosheets were conducive to electron rapid transfer achieving the enhanced CO_2RR activity.

In addition to using 2D COFs as the electrocatalyst for carbon dioxide electroreduction alone, integrating 2D COFs with other excellent conductive materials can also solve the issue of poor

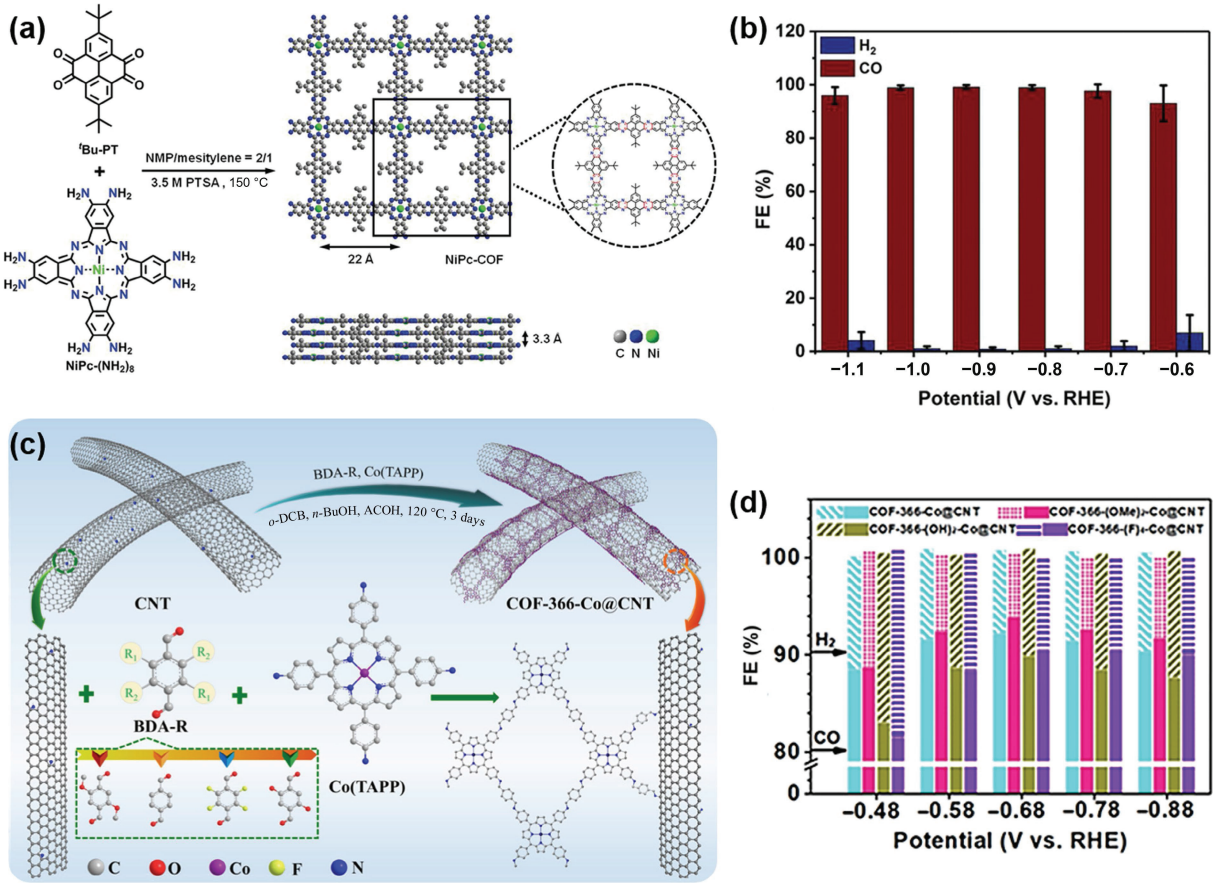

Figure 11 (a) Schematic illustration for the synthesis of 2D conductive NiPc-COF. (b) FE_{CO} and FE_{H2} of NiPc-COF in CO_2-saturated 0.5 M $KHCO_3$ electrolyte. Reproduced with permission from Ref. [130], © Wiley-VCH GmbH 2020. (c) Schematic illustration for the synthesis of cobalt porphyrin-based COF. (d) FEs. Reproduced with permission from Ref. [219], © American Chemical Society 2020.

conductivity. Lu et al. [219] fabricated a series of composite materials by the template-oriented polymerization of COFs grafted on amino-functionalized carbon nanotubes (CNTs) as conductive scaffolds (Fig. 11(c)). The thickness of as-prepared COF nanolayers was only 0.9 nm and the distance from COF to the conductive scaffold was drastically shortened. As for electrocatalytic CO_2RR performances, COF-366-$(OMe)_2$-Co@CNT displayed outstanding selectivity of CO_2 conversion to CO with the highest FE of 93.6% at −0.68 V. Furthermore, the total current density of COF-366-$(OMe)_2$-Co@CNT reached up to 40 mA·cm^{-2} at −1.05 V and the total current densities all exhibited a favorable stability at the potentials from −0.53 to −0.88 V kept for 2,700 s. In order to access the catalytic activity, the TOF values in Fig. 11(d) of the four samples were calculated, and the results manifested COF-366-$(OMe)_2$-Co@CNT owned the highest TOF values 11,877 h^{-1} at the overpotential of 0.77 V. Meanwhile, COF-366-$(OMe)_2$@CNT without Co centers and COF-366-$(OMe)_2$-Co without CNTs were synthesized to identify the active sites for CO_2RR and COF-366-$(OMe)_2$@CNT, which exhibited the best performance in terms of the current densities and CO selectivity.

4.2 HER

Along with ever-growing environmental issues, hydrogen gas as a clean energy has a great application prospect and thus electrochemical HER as an important pathway to generate H_2 attracts a lot of attention. Transition metal-based compounds have been widely applied as HER catalysts. However, several obstacles including the corrosion of metal, poor stability, undesirable catalytic activity, and high cost impede their development. Therefore, diverse 2D COFs with multiple advantages mentioned above become promising substitutes of transition metal-based compounds as HER electrocatalysts in the near future.

Maiti et al. [220] synthesized a 2D COF by the reaction between the 3,4-diaminobenzohydrazide and benzene-1,3,5-tricarboxaldehyde, and adopted the 2D COF to encapsulate metal Ru to enhance the stability and catalytic activity of this 2D COF loaded Ru (Ru@COF) (Figs. 12(a) and 12(b)). The as-prepared Ru@COF showed an efficient HER activity with an ultralow overpotential of 212 mV at a current density of 10 mA·cm^{-2}. Because a lower Tafel slope value reflects faster catalytic reaction, in Fig. 12(c), the Tafel slope of 79 mV·dec^{-1} for Ru@COF catalyst was much lower than pure Ru (137 mV·dec^{-1}) or pure COF (180 mV·dec^{-1}), indicating the capacity of faster electrode reaction. As for the stability of Ru@COF, there was almost no decay in current density and onset overpotential, indicating its good stability.

Heteroatoms-doping engineering is an efficient method to modulate electronic structure of carbon-based electrocatalysts. Therefore, except the utilization of as-synthesized pristine COFs as the electrocatalysis for HER, Yang et al. [221] reported N, P co-doped porous carbons derived from nanoporous 2D COFs by the carbonization and phosphorization, and four types of N and P co-doped carbons (1"-NP, 2"-NP, 3"-NP, and 4"-NP) were prepared through the reaction between 1,3,6,8-tetrakis(4-aminophenyl)pyrene (TAP)/1,2,4,5-tetrakis(4-aminophenyl) benzene (TAB) and 1,2,4,5-tetrakis(4-formylphenyl)-benzene (TFB)/1,2,4,5-tetrakis(4-formylphenyl)-3,6-dimethyl-benzene (TFDB) (Fig. 12(d)). In alkaline electrolyte, 1"-NP exhibited the highest ORR activity was attributed to the formation of graphitic N atoms and plentiful P atoms. More specifically, the Tafel slope in Fig. 12(e) of 1"-NP (70 mV·dec^{-1}) was lower than that of 2"-NP (131 mV·dec^{-1}), 3"-NP (124 mV·dec^{-1}), 4"-NP (87 mV·dec^{-1}), and even than that of Pt/C (117 mV·dec^{-1}). In the tests of HER activity in Ar-saturated 1.0 M $HClO_4$ solution, 1"-NP showed the lowest overpotential of ~ 260 mV at 10 mA·cm^{-2} and achieved a Tafel slope of ~ 175 mV·dec^{-1} in Fig. 12(f). The good stability was reflected from the unchanged polarization curve of 1"-NP after 10,000 cycles. The enhanced activity and stability were contributed to the increased edge effects and stabilized C–N species by P doping. It is worth mentioning that as-prepared N, P co-doped porous carbons are also endowed with ORR activity.

4.3 OER

OER as another half reaction is the rate-determining step of the water splitting. Different from the two-electron transfer reaction in the HER, OER involves four protons and electron-coupled reaction and thus its process has sluggish kinetics. Therefore, this reaction process needs a huge overpotential to drive. The design and synthesis of efficient OER catalysts are very significant to improve the energy efficiency of water electrolysis.

Mondal et al. [222] synthesized a thiadiazole-based imine-linked COF (C4-SHz COF) by the general Schiff base condensation polymerization between 1,3,5-tris(4-formylphenyl)benzene (C4-CHO) and 2,5-dihydrazinyl-1,3,4-

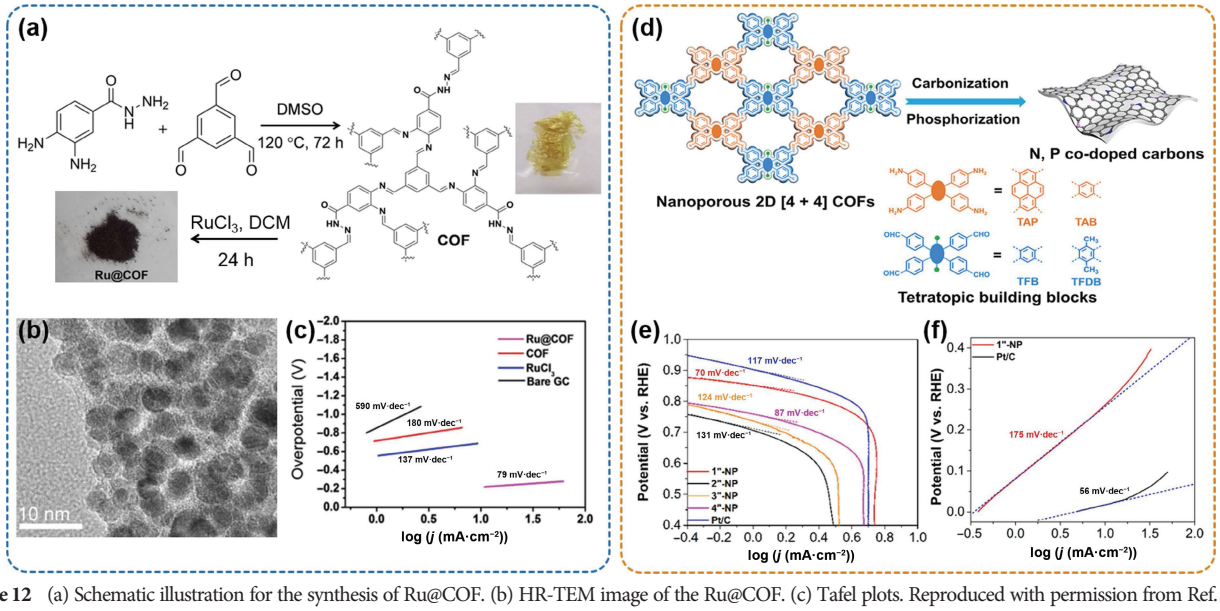

Figure 12 (a) Schematic illustration for the synthesis of Ru@COF. (b) HR-TEM image of the Ru@COF. (c) Tafel plots. Reproduced with permission from Ref. [220], © Wiley-VCH Verlag GmbH & Co. KGaA, Weinheim 2019. (d) Schematic illustration for the synthesis of N, P-doped carbons. (e) Tafel plots. (f) Tafel curves of 1"-NP and Pt/C. Reproduced with permission from Ref. [221], © American Chemical Society 2020.

thiadiazole (SHz) under the solvothermal reaction for 36 h (Fig. 13(a)). The calculated BET surface area of as-obtained COF (C4-SHz COF) was 1,224 $m^2 \cdot g^{-1}$. As LSV curves recorded in Fig. 13(b), C4-SHz COF owned high activity with a low overpotential of 320 mV at the current density of 10 $mA \cdot cm^{-2}$ and the overpotential was lower than the benchmark catalyst IrO_2/C. Besides, a lower Tafel slope value (39 $mV \cdot dec^{-1}$) for C4-SHz COF in comparison with IrO_2/C (57 $mV \cdot dec^{-1}$) indicated its splendid electrocatalytic activity in Fig. 13(c). At the current density of 10 $mA \cdot cm^{-2}$, the chronopotentiometry measurements were conducted to analyze the long-term durability of the C4-SHz COF in Fig. 13(d), and the results indicated that it could efficiently work for more than 11 h (Fig. 13(e)).

Using 2D layered COFs as the supporting materials to disperse metal NPs showed positive results, and thus integrating COFs with metal-based materials is another effective strategy to improve catalytic performance of OER. Nandi et al. [223] grew Ni_3N on the low band gap benzimidazole COF via nanoscopic confinement, and the low band gap substrates with delocalized conjugated π-electrons are very suitable as ideal electronic supports (Fig. 14(a)). In the actual electrochemical performance (Figs. 14(b) and 14(c)), the overpotential (η) of the composite was 230 mV at 10 $mA \cdot cm^{-2}$ and a Tafel slope value of 79 $mV \cdot dec^{-1}$ indicated the capacity of efficient mass and charge transfer. At the current density of 1 $mA \cdot cm^{-2}$, FE was 98% and it reduced to 58% at 10 $mA \cdot cm^{-2}$. Besides, almost no change in the cyclic voltammetry of the composites was found at 50 $mA \cdot s^{-1}$ after the 500 cycles, indicating a stable catalytic performance.

Generally speaking, electrocatalytic activity of the metal-based electrocatalysts is better than the metal-free materials. The nitrogen-doping engineering is promising to change this fact by directly inducing uneven charge distribution of C atoms to create more active sites. Featuring with chemical stability, porous structures, and accurate introduction of N atoms, 2D COFs are known as a wonderful candidate. Based on the previous works, Yang et al. [16] synthesized the COF-C_4N by the solvothermal reaction of triphenylenehexamine and hexaketocyclohexane as shown in Fig. 14(d). Different from taking the place of each double bond in graphene with four fused phenazine-linked rings for COF-C_4N, three or five fused phenazine-linked rings of h-C_2N and h-C_5N_2 were at location of double bond in graphene. In catalytic performance tests, the overpotential (η) calculated for COF-C_4N was 349 mV at 10 $mA \cdot cm^{-2}$, and its Tafel slope was 64 $mV \cdot dec^{-1}$, indicating it owned efficient charge transfer at the electrode–electrolyte contacts (Fig. 14(e)). Besides, the overpotential (η) values of h-C_2N and h-C_5N_2@1M were 546 and 508 mV at 10 $mA \cdot cm^{-2}$, which were higher than COF-C_4N. For assessing the electrochemical stability, the results of

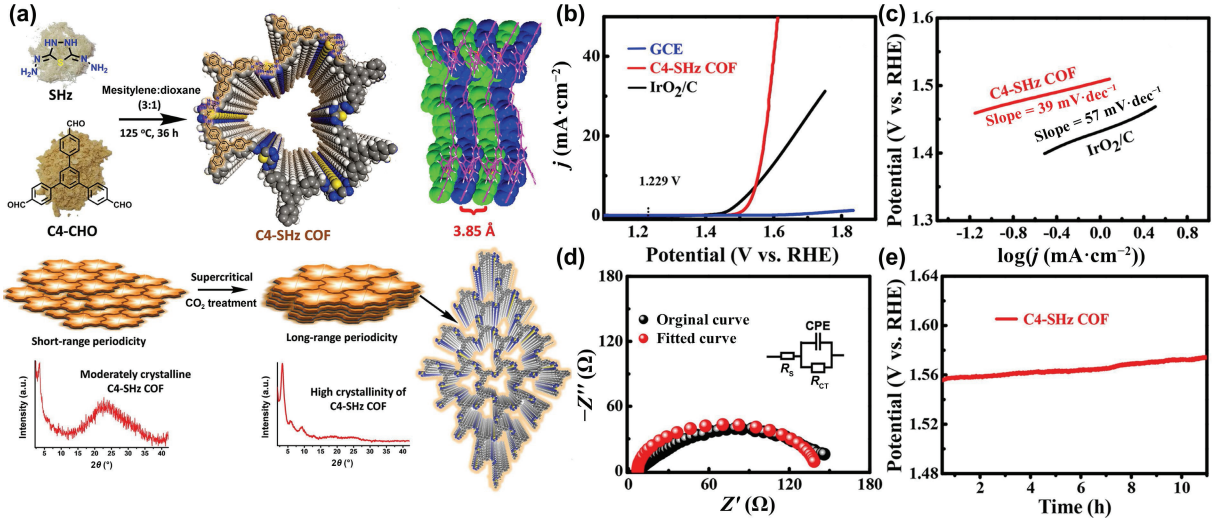

Figure 13 (a) Schematic illustration for the synthesis of C4-SHzCOF. (b) LSV curves. (c) Tafel plots of C4-SHzCOF and IrO_2/C. (d) Nyquist plots. (e) The stability test. Reproduced with permission from Ref. [222], © American Chemical Society 2020.

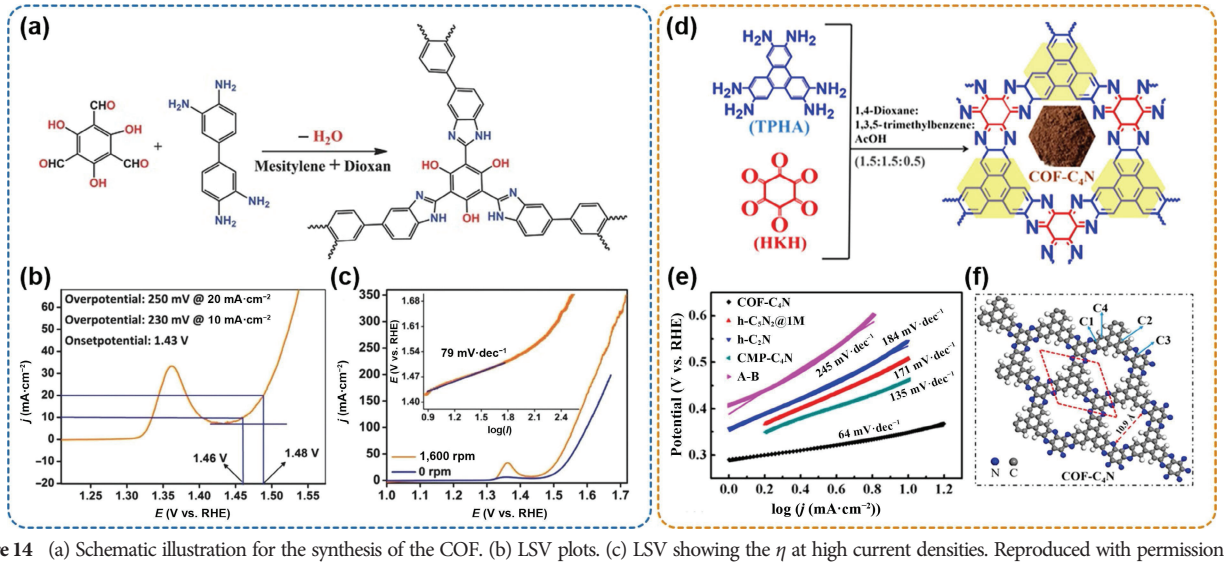

Figure 14 (a) Schematic illustration for the synthesis of the COF. (b) LSV plots. (c) LSV showing the η at high current densities. Reproduced with permission from Ref. [223], © WILEY-VCH Verlag GmbH & Co. KGaA, Weinheim 2016. (d) Schematic illustration for the synthesis of COF-C_4N. (e) Tafel plots. (f) Structure diagrams of COF-C_4N. Reproduced with permission from Ref. [16], © American Chemical Society 2019.

chronoamperometry measurements with the 83.61% of catalytic current density kept after 20 h. Additionally, it was also proven that the OER performance of crystalline material COF-C_4N was better than that of amorphous material CMP-C_4N prepared by the similar routine as COF-C_4N. The C_4 sites at the edge in Fig. 14(f) were thought to be more suitable active sites due to easier electron/holes transfer than other sites.

4.4 ORR

The ORR is widely applied in the fields of fuel cells and rechargeable metal–air batteries. The most familiar catalyst for ORR is high-cost noble metal like Pt, and thus developing cost-effective as well as high-performance catalyst is necessary. In terms of fuel cells, metal Pt is regarded as a sort of highly efficient metal catalysts [224, 225] and researches on Pt-based carbon materials have been widely reported. In order to enhance the utilization efficiency of noble metals on carbon materials and lower costs, 2D COFs were chosen as the supporting materials to solve the problem of the large-scale production. Zhai et al. [132] chose 2,4,6-trimethyl-1,3,5-trizaine (TM) and 1,3,5-tris-(4-formylphenyl)-triazine (TPT) to synthesize TM-TPT-COF, and subsequently as-prepared COF was impregnated in a $K_2[PtCl_4]$ solution to obtain the final production Pt@COF (Figs. 15(a)–15(c)). Pt@COF exhibited a higher catalytic activity with a more positive E_0 of 1.04 V and $E_{1/2}$ of 0.89 V, which were 70 and 60 mV than that of Pt/C, respectively (Fig. 15(d)). As shown in Fig. 15(e), the electron-transfer numbers (n values) of Pt@COF were from 3.9 to 4 with the potential range from 0.2 to 0.8 V, manifesting a direct $4e^-$ mechanism dominating the ORR process. The electrochemical impedance spectroscopy revealed that Pt loaded on the COF can be conducive to the electron transfer. After 50 h, around 95% of the current density of Pt@COF was remained, demonstrating an excellent long-term stability.

The utilization of 2D heteroatom-doped carbon materials synthesized by COFs as ORR catalysts is an indirect application of 2D COF in the field of electrocatalysis. On account of the direct pyrolysis of COFs resulting in the loss of 2D porous structures, Xu et al. [226] proposed a new idea to transform COFs into 2D carbons with the assistance of phytic acid (PA) as a template (Figs. 15(f) and 15(g)). PA@TAPT-DHTA-COF was prepared by the condensation of 4,4',4"-(1,3,5-triazine-2,4,6-triyl)trianiline (TAPT) and 2,5-dihydroxyterephthalaldehyde (DHTA) via solvothermal method. Thereinto, PA can not only exfoliate the layered 2D COFs into small-sized carbon sheets and guide the conversion of its layers into 2D carbons, but also introduce phosphorus atoms into carbon skeleton and promote the formation of porous structure. TAPT-DHTA-COF_{1000} without PA had a relatively low activity for catalyzing ORR with an onset potential (E_O) of −0.12 V, halfwave potential ($E_{1/2}$) of −0.29 V, and diffusion limiting current density (j_{limit}) of 4.0 mA·cm^{-2} (Fig. 15(h)). Notably, PA@TAPT-DHTA-COF_{1000} obtained an E_0 value at −0.02 V, $E_{1/2}$ at −0.19 V, and j_{limit} at 6.5 mA·cm^{-2}, respectively. On the basis of PA@TAPT-DHTA-COF_{1000}, it was further modified by pyrolyzing in ammonia atmosphere to synthesis PA@TAPT-DHTA-$COF_{1000NH3}$. As for ORR activity, the Tafel slope of PA@TAPT-DHTA-$COF_{1000NH3}$ (110 mV·dec^{-1}) was much smaller than PA@TAPT-DHTA-COF_{1000} (146 mV·dec^{-1}) or Pt/C (121 mV·dec^{-1}), demonstrating a superior ORR activity for PA@TAPT-DHTA-$COF_{1000NH3}$ (Fig. 15(i)). PA@TAPT-DHTA-$COF_{1000NH3}$ with 95% of the original current density retained after 5.5 h exhibited its outstanding durability property. It was found that the introduction of ammonia provided more active sites for PA@TAPT-DHTA-$COF_{1000NH3}$ and regulated the porous

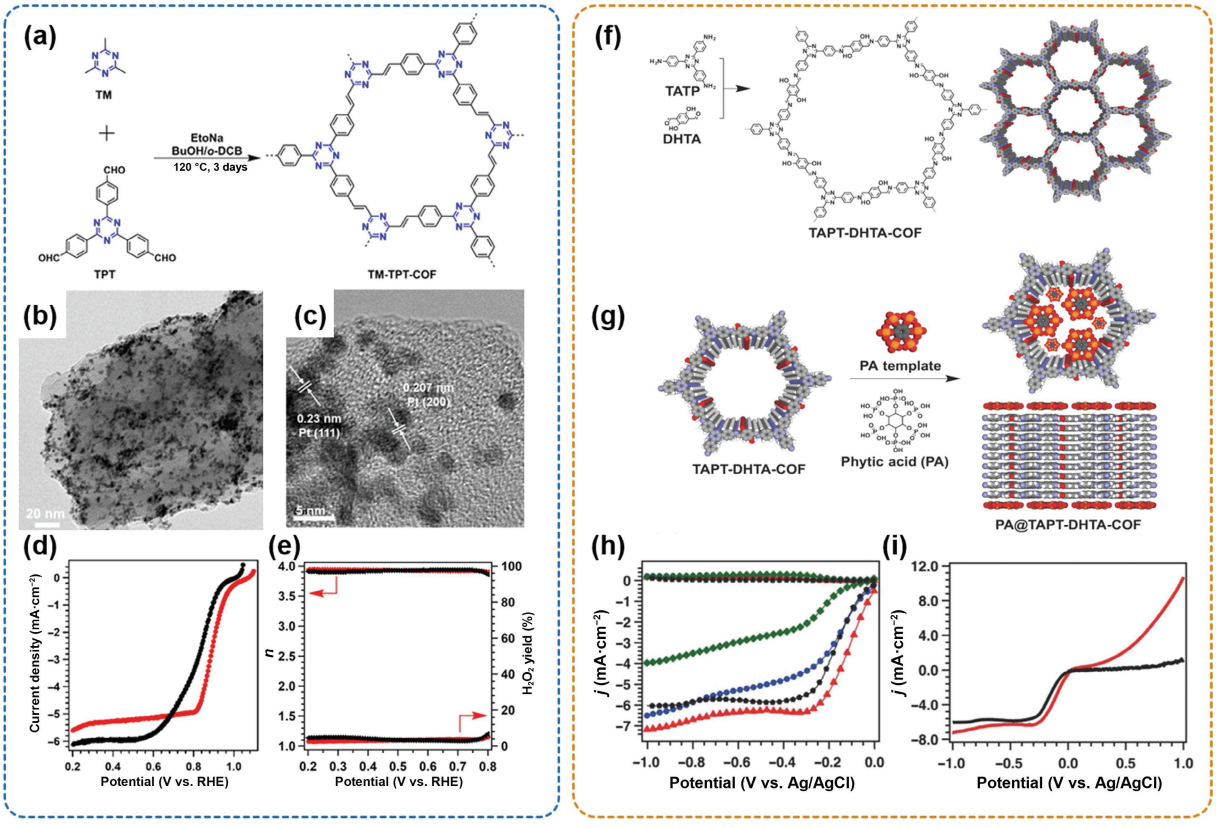

Figure 15 (a) Schematic illustration for the synthesis of the TM-TPT-COF. (b) HR-TEM image of Pt@COF. (c) HR-TEM image of Pt NPs in Pt@COF. (d) LSV curves of Pt@COF (red) and Pt/C (black). (e) Electron-transfer number (n) and H_2O_2 yield plots for Pt@COF (red) and Pt/C (black). Reproduced with permission from Ref. [132], © American Chemical Society 2020. (f) and (g) Schematic illustration for the synthesis of the TAPT-DHTA-COF and PA@TAPT-DHTA-COF. (h) Rotating ring disk electrode (RRDE) profiles of TAPT-DHTA-COF_{1000} (green), PA@TAPT-DHTA-COF_{1000} (blue), PA@TAPT-DHTA-$COF_{1000NH3}$ (red), and Pt/C (black) electrodes. (i) LSV curves of PA@TAPT-DHTA-$COF_{1000NH3}$ (red) and Pt/C (black). Reproduced with permission from Ref. [226], © WILEY-VCH Verlag GmbH & Co. KGaA, Weinheim 2018.

structure.

The spontaneous stacking of 2D COFs can decrease the exposed active sites, leading to bad ORR electrocatalytic performance. Constructing 2D COFs as the coating layer of conductive materials is likewise a feasible method to solve the problem of spontaneous stacking and low electron transfer rate of 2D COF nanosheets. Liu et al. [227] successfully synthesized a nanohybrids of 2D-COFs and CNTs with coaxial one-dimensional van der Waals heterostructures (CC-*X* vdWHs, *X*: the thickness of the COF shell). As Fig. 16(a) shown, the 2D-COF (TAPTt-COF) was constructed via 4,4',4",4"'-(pyrene-1,3,6,8-tetrayl)tetraaniline (TTAP) and thieno [3,2-b]thiophene-2,5-dicarboxaldehyde (TtDCA). Actually, the thickness of the COF shell can be precisely adjusted and influences the electrocatalytic activity of CC-*X* vdWHs for both ORR. As for the actual electrocatalytic performances of ORR, CC-3 possessed the highest ORR activity with the highest $E_{1/2}$ of 0.828 V (pristine TAPTt-COF: 0.741 V, CNTs: 0.698 V, the physical mixture of TAPTt-COF and CNT: 0.761 V). The electron transfer number (n) of CC-3 was around 3.86 following a stable 4e⁻ ORR pathway (Fig. 16(a)). The mass-normalized kinetic current density ($j_{K\text{-mass}}$) decreased with the increased thickness of COF shell. Due to the thinnest thickness, CC-2 owned the highest $j_{K\text{-mass}}$ (1.01 A·mg^{-1}), but CC-3 achieved a better overall catalytic performance for ORR. After 24 h (Fig. 16(b)), 94% of the initial current density retained showed a better stability for CC-3 than Pt/C (76%).

In addition, CC-3 also performed well for OER in 0.1 M KOH electrolyte. It manifested the best catalytic performance with the lowest overpotential (η) of 389 mV and relatively low Tafel slopes (101 mV·dec^{-1}) in Fig. 16(c). The TOF of these samples was calculated and CC-2 obtained a slightly higher TOF value (0.138 s^{-1}) than CC-3 (0.134 s^{-1}), showing higher intrinsic activity for CC-2. In the chrono potentiometric stability test, only less than 4% overpotential increment was found with excellent stability (Fig. 16(d)). This experiment demonstrated the carbon-sulfur regions in thienothiophene groups of this 2D-COF were active catalytic center for ORR and OER.

4.5 NRR

In the field of chemical NH_3 production, traditional Haber–Bosch process ($N_2 + 3H_2 \rightarrow 2NH_3$, $\Delta H_{298\ K} = -92.2$ kJ·mol^{-1}) has been extensively used for a long time, but it still has a lot of shortcomings, such as the energy consumption and large-scale emissions of greenhouse gases (Fig. 17) [228]. In order to deal with these problems and meet the sustainable development, researchers pay more attention to the electrocatalytic N_2 fixation (NRR, $2N_2 + 6H_2O \rightarrow 4NH_3 + 3O_2$) as the substitute of Haber–Bosch process under the help of renewable electricity.

Theoretically, choosing H_2O as the proton source to produce NH_3 under room temperature and atmospheric pressure is feasible and can effectively solve energy crisis and CO_2 emission. However, there are many challenges in practical NRR process. On the one hand, either direct reduction or activation for N_2 is hard, demonstrating a low activity is one challenge for electrocatalytic

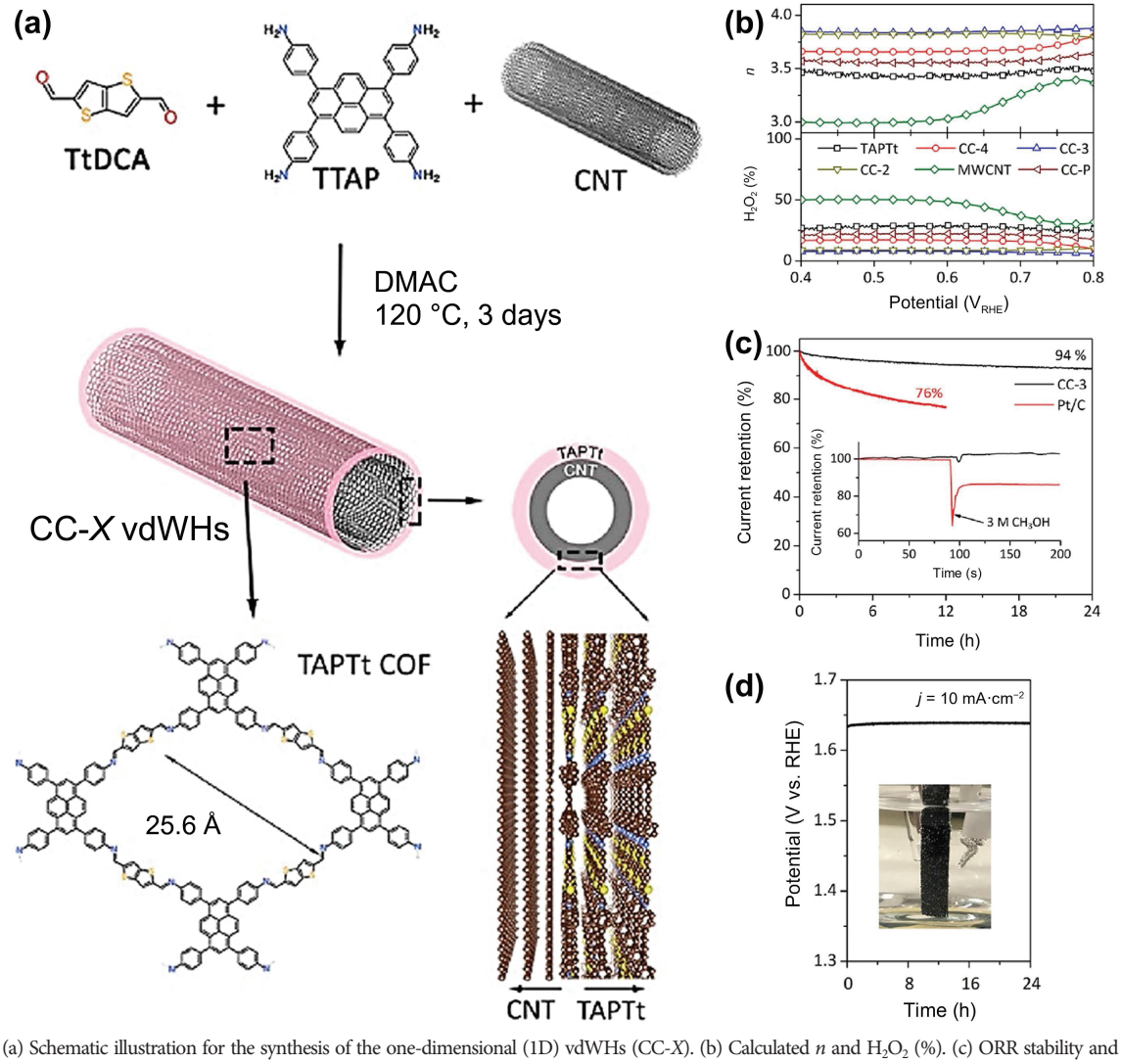

Figure 16 (a) Schematic illustration for the synthesis of the one-dimensional (1D) vdWHs (CC-*X*). (b) Calculated n and H_2O_2 (%). (c) ORR stability and methanol tolerance test (inset) of CC-3. (d) OER stability of CC-3. Reproduced with permission from Ref. [227], © American Chemical Society 2021.

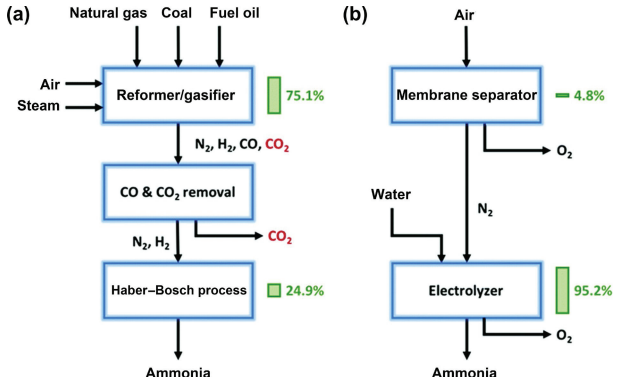

Figure 17 The share of the total energy input of (a) Haber–Bosch process and (b) electrochemical process for NH_3 synthesis. Reproduced with permission from Ref. [228], © The Royal Society of Chemistry 2021.

N_2 fixation. On the other hand, there is a competitive reaction between NRR and HER, indicating the importance of selectivity. Thus, it is highly desirable to develop the high-performance catalysts with excellent catalytic activity and selectivity for NRR.

By heteroatom-doping strategy, carbon frameworks introduced by boron atoms can generate electron deficiency, resulting in enhanced electrocatalytic activity. COFs linked by boronate ester (C_2O_2B) or boroxine rings (B_3O_3) with a large number of B atoms have the feature of Lewis acidity that can effectively promote the N_2 (a weak Lewis base) adsorption. Considering the poor electrical conductivity of COFs, Liu et al. [122] synthesized boron-rich COFs grown on the N-doped carbon nanosheets (COF/NC) by molecular dehydration reaction of 1,4-benzenediboronic acid (BDBA), and electrochemically excitated COF/NC (Eex-COF/NC) was obtained via potentiostatic electrolyzing (Fig. 18(a)). In the actual electrocatalytic nitrogen reduction performance of Eex-COF/NC (Fig. 18(b)), the FE and NH_3 yield rate of Eex-COF/NC achieved the maximum value of 45.43% and 12.53 $\mu g \cdot h^{-1} \cdot mg^{-1}$, respectively, at −0.2 V vs. RHE. As shown in Figs. 18(c) and 18(d), the results showed that the majority of electrons trended to NH_3 yield rather than HER in the voltage range from −0.1 to −0.3 V vs. RHE. Besides, Eex-COF/NC exhibited a robust stability with unchanged performance after 10 cycles of NRR electrolysis (Fig. 18(e)). An extra experiment proved that the feeding gas rather than any nitrogen species of NC provided the N source. Molecular dynamics simulation snapshots (Figs. 18(f)–18(h)) indicated a good affinity with more N_2 molecules existing around the Eex-COF in comparison with pristine COF. The formation of B–N bonds distorted the lattice planes of COFs and significantly promoted the ability of N_2 adsorption.

From the computational simulation point of view, Wang et al. [229] employed the robust linkage between 2,3,9,10,16,17,23,24-octaamino-metallophthalocyanine and pyrene-4,5,9,10-tetraone to construct a series of 2D conductive TM-based COFs (TM-COFs, TM = Sc, Ti, V, Cr, Mn, Fe, Co, Ni, Cu, Zn, Nb, Mo, Ru, Rh, Pd, Ag, W, Ir, Pt, and Au, respectively) based on DFT. Among TM-COFs, Mn, Co, Ni, Zn, and Ag-COF with a positive ΔG values of N_2 adsorption are unfavorable for N_2 fixation due to poor behaviors for N_2 activation. Also, Ti-, V-, Cr-, Nb-, Mo-, and W-COF were considered as potential NRR candidates and Mo-COF owned the lowest ΔG_{PDS} (PDS: potential-determining steps) value of 0.28 eV and a very low overpotential of 0.16 V. In Mo-COF, the Mo site with positive charge made itself unsuitable for HER. The simulation results indicated that the FE NRR value is close to

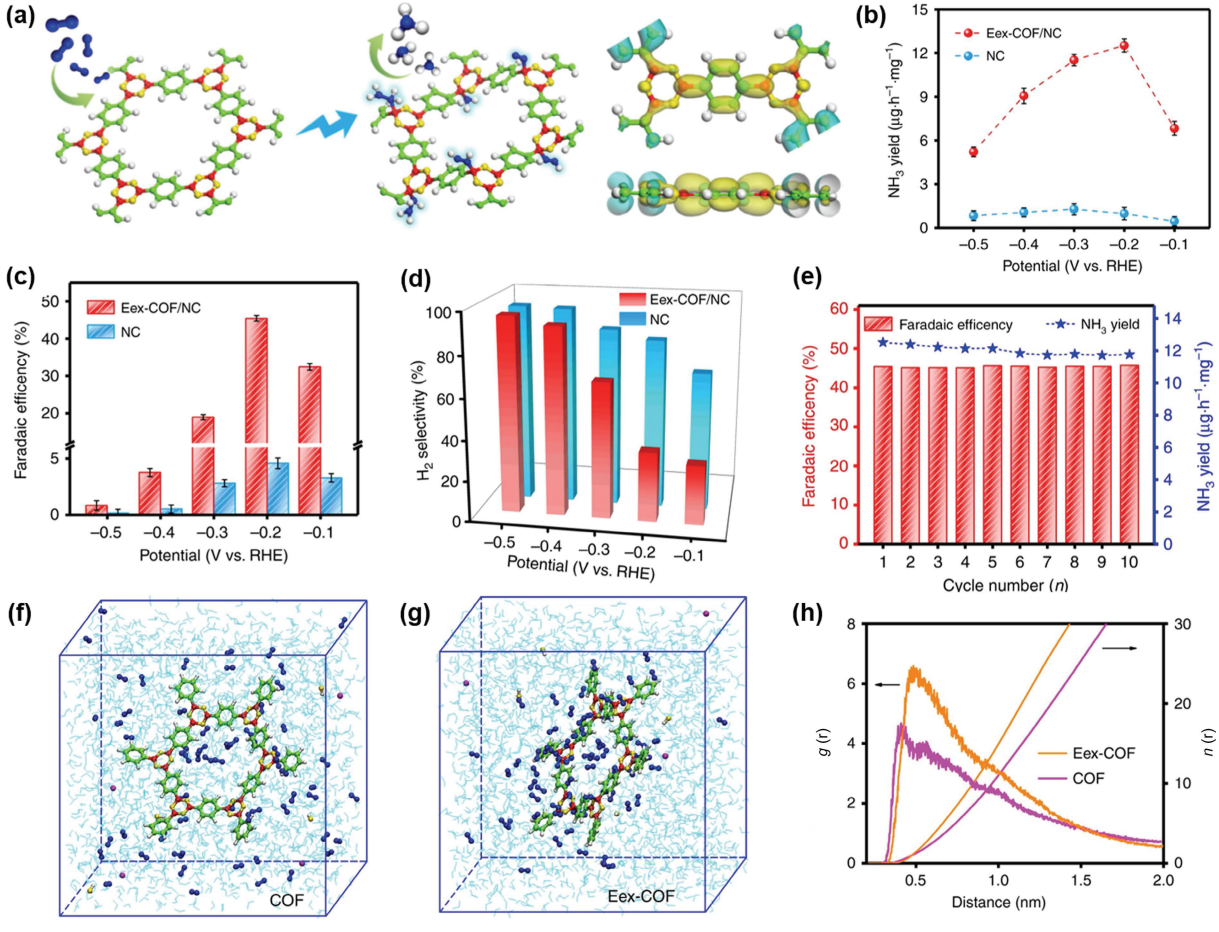

Figure 18 (a) Schematic illustration of the electrochemical excitation of COF. (b) NH_3 yield rates at the different potentials. (c) FEs and (d) H_2 selectivity of Eex-COF/NC. (e) The durability test of Eex-COF/NC. (f) and (g) Molecular dynamics simulation snapshots of (f) COF and (g) Eex-COF. (h) Radial distribution function (RDF) and integrated RDF of nitrogen molecules around different models. Reproduced with permission from Ref. [122], © Liu, S. S. et al. 2019.

100% for Mo-COF and thermal stability with no geometrical distortion for Mo-COF in the 10 ps simulation.

5 The challenges and opportunities of 2D COFs in electrocatalysis

In conclusion, we briefly overview the development status of 2D COFs applied in diverse electrocatalysis fields. Up to now, the related researches are still scarce, and more types of active centers, building blocks, and linkages in 2D COFs are expected to continue to explore. Compared with the conventional metal catalysts, 2D COFs have stronger designability and higher stability in structure and performance. However, the current COF-based electrocatalysts are far from the industrial and commercial applications, and good conductivity, as well as abundant active sites, is unambiguous orientations for the design and preparation. Based on this, the major challenges toward further development and the modification methods to endow 2D COFs based-materials with outstanding electrocatalytic performance are featured as the following aspects:

(1) From the perspective of synthesis, most 2D COFs are prepared by harsh solvothermal approaches, which demand more energy and prevent their massive production [230]. Although some existing researches have been carried out on the synthesis at ambient temperature and pressure [231], there are few synthetic methods that are suitable for most types of linkages. Therefore, more studies should focus on investigating general energy-saving commercial synthetic strategies.

(2) Conductivity is a critical characteristic of electrocatalysts, and a change in current density may affect local reaction environment [232], which induces the transformation of common products. Moreover, high current density means a high rate of the desired production and a profitable capital expenditure [233]. Unfortunately, few of the 2D COF-based catalysts previously reported deal with industrially relevant current densities (> 200 mA·cm^{-2}). By rationally designing the building blocks with the increasing planarity and the extended π conjugation (such as phthalocyanine), highly efficient conductive porous framework materials for electrocatalysis were synthesized. Utilization of the derived carbon materials or mix of 2D COFs and some conductive materials (e.g., CNT and nano-micro carbon sphere) can ameliorate the self-stacking and open the intrinsic bandgap in favor of electron rapid transfer. The reduction of layer thickness can provide increasing contact with conductive materials and improve their conductivity [234]. In addition, the increasing loadings also alleviate this existing problem [235].

(3) In the electrochemical CO_2 reduction, multicarbon products are regarded as high-energy-density and high-value-added. Regretfully, few 2D COFs are active for C_2 formation. Hence, we should devote to adopting doping-engineering, synergistically introducing active centers for the tandem catalysis [236], precisely controlling their structures, and tailoring the composites to enhance the deep reduction products and promote the favor for C_2 products on 2D COF electrocatalysts.

In summary, the development for 2D COFs based materials has been encouraging and fascinating [237, 238], not just the substrates supporting noble metals but as the promising highly efficient catalysts. Improving the selectivity and partial current density of high-value-added product is unambiguous orientation for the design and preparation of 2D COFs. Thereinto, computation-aided simulations are still demanded to predict the activity of new materials and further reveal the real reason that the novel 2D COFs after modification dramatically enhanced the electrocatalytic performances for each research. Although the research on the electrocatalytic application of 2D COFs still faces tremendous challenges, we believe that the discovery of novel 2D COF catalysts and properties will be unstoppable.

Acknowledgements

This project was supported by the National Natural Science Foundation of China (Nos. 22071172, 21872103, and 52073208).

References

[1] Zhang, J. K.; Tian, W. S.; Chipperfield, M. P.; Xie, F.; Huang, J. L. Persistent shift of the Arctic polar vortex towards the Eurasian continent in recent decades. *Nat. Climate Change* **2016**, *6*, 1094–1099.

[2] Coumou, D.; Di Capua, G.; Vavrus, S.; Wang, L.; Wang, S. The influence of Arctic amplification on mid-latitude summer circulation. *Nat. Commun.* **2018**, *9*, 2959.

[3] Shindell, D.; Smith, C. J. Climate and air-quality benefits of a realistic phase-out of fossil fuels. *Nature* **2019**, *573*, 408–411.

[4] Du, J.; Li, F.; Sun, L. C. Metal–organic frameworks and their derivatives as electrocatalysts for the oxygen evolution reaction. *Chem. Soc. Rev.* **2021**, *50*, 2663–2695.

[5] Li, L. G.; Wang, P. T.; Shao, Q.; Huang, X. Q. Metallic nanostructures with low dimensionality for electrochemical water splitting. *Chem. Soc. Rev.* **2020**, *49*, 3072–3106.

[6] Tang, T. M.; Li, S. S.; Sun, J. R.; Wang, Z. L.; Guan, J. Q. Advances and challenges in two-dimensional materials for oxygen evolution. *Nano Res.* **2022**, *15*, 8714–8750.

[7] Zaman, S.; Huang, L.; Douka, A. I.; Yang, H.; You, B.; Xia, B. Y. Oxygen reduction electrocatalysts toward practical fuel cells: Progress and perspectives. *Angew. Chem., Int. Ed.* **2021**, *60*, 17832–17852.

[8] Asset, T.; Atanassov, P. Iron-nitrogen-carbon catalysts for proton exchange membrane fuel cells. *Joule* **2020**, *4*, 33–44.

[9] Liu, Q. Q.; Liu, R. T.; He, C. H.; Xia, C. F.; Guo, W.; Xu, Z. L.; Xia, B. Y. Advanced polymer-based electrolytes in zinc–air batteries. *eScience* **2022**, *2*, 453–466.

[10] Li, J. J.; Zhang, Z. C.; Hu, W. P. Insight into the effect of metal cations in the electrolyte on performance for electrocatalytic CO_2 reduction reaction. *Energy Environ. Mater.* **2022**, *5*, 1008–1009.

[11] Gu, J. W.; Peng, Y.; Zhou, T.; Ma, J.; Pang, H.; Yamauchi, Y. Porphyrin-based framework materials for energy conversion. *Nano Res. Energy* **2022**, *1*, e9120009.

[12] Hou, M.; Shi, Y. X.; Li, J.; Gao, Z. Q.; Zhang, Z. C. Cu-based organic–inorganic composite materials for electrochemical CO_2 reduction. *Chem. Asian J.* **2022**, *17*, e202200624.

[13] He, T.; Yang, C. H.; Chen, Y. Z.; Huang, N.; Duan, S. M.; Zhang, Z. C.; Hu, W. P.; Jiang, D. L. Bottom-up interfacial design of covalent organic frameworks for highly efficient and selective electrocatalysis of CO_2. *Adv. Mater.* **2022**, *34*, 2205186.

[14] Wang, C. Y.; Zhang, Z. C.; Zhu, Y. T.; Yang, C. H.; Wu, J. S.; Hu, W. P. 2D covalent organic frameworks: From synthetic strategies to advanced optical-electrical-magnetic functionalities. *Adv. Mater.* **2022**, *34*, 2102290.

[15] El-Kaderi, H. M.; Hunt, J. R.; Mendoza-Cortes, J. L.; Cote, A. P.; Taylor, R. E.; O'Keeffe, M.; Yaghi, O. M. Designed synthesis of 3D covalent organic frameworks. *Science* **2007**, *316*, 268–272.

[16] Yang, C. H.; Yang, Z. D.; Dong, H.; Sun, N.; Lu, Y.; Zhang, F. M.; Zhang, G. L. Theory-driven design and targeting synthesis of a highly-conjugated basal-plane 2D covalent organic framework for metal-free electrocatalytic OER. *ACS Energy Lett.* **2019**, *4*, 2251–2258.

[17] Aiyappa, H. B.; Thote, J.; Shinde, D. B.; Banerjee, R.; Kurungot, S. Cobalt-modified covalent organic framework as a robust water oxidation electrocatalyst. *Chem. Mater.* **2016**, *28*, 4375–4379.

[18] Mazloomi, S. K.; Sulaiman, N. Influencing factors of water electrolysis electrical efficiency. *Renew. Sustain. Energy Rev.* **2012**, *16*, 4257–4263.

[19] Lin, C. Y.; Zhang, D. T.; Zhao, Z. H.; Xia, Z. H. Covalent organic

framework electrocatalysts for clean energy conversion. *Adv. Mater.* **2018**, *30*, 1703646.
[20] Yusran, Y.; Fang, Q. F.; Valtchev, V. Electroactive covalent organic frameworks: Design, synthesis, and applications. *Adv. Mater.* **2020**, *32*, 2002038.
[21] Qu, L. T.; Liu, Y.; Baek, J. B.; Dai, L. M. Nitrogen-doped graphene as efficient metal-free electrocatalyst for oxygen reduction in fuel cells. *ACS Nano* **2010**, *4*, 1321–1326.
[22] Deng, D. H.; Pan, X. L.; Yu, L.; Cui, Y.; Jiang, Y. P.; Qi, J.; Li, W. X.; Fu, Q.; Ma, X. C.; Xue, Q. K. et al. Toward N-doped graphene via solvothermal synthesis. *Chem. Mater.* **2011**, *23*, 1188–1193.
[23] Li, Y. F.; Zhou, Z.; Shen, P. W.; Chen, Z. F. Spin gapless semiconductor–metal–half-metal properties in nitrogen-doped zigzag graphene nanoribbons. *ACS Nano* **2009**, *3*, 1952–1958.
[24] Wang, Y. S.; Chen, J. X.; Wang, G. X.; Li, Y.; Wen, Z. H. Perfluorinated covalent triazine framework derived hybrids for the highly selective electroconversion of carbon dioxide into methane. *Angew. Chem., Int. Ed.* **2018**, *57*, 13120–13124.
[25] Hao, L.; Zhang, S. S.; Liu, R. J.; Ning, J.; Zhang, G. J.; Zhi, L. J. Bottom-up construction of triazine-based frameworks as metal-free electrocatalysts for oxygen reduction reaction. *Adv. Mater.* **2015**, *27*, 3190–3195.
[26] Li, D. H.; Li, C. Y.; Zhang, L. J.; Li, H.; Zhu, L. K.; Yang, D. J.; Fang, Q. R.; Qiu, S. L.; Yao, X. D. Metal-free thiophene-sulfur covalent organic frameworks: Precise and controllable synthesis of catalytic active sites for oxygen reduction. *J. Am. Chem. Soc.* **2020**, *142*, 8104–8108.
[27] Qian, H. L.; Li, Y.; Yan, X. P. A building block exchange strategy for the rational fabrication of de novo unreachable amino-functionalized imine-linked covalent organic frameworks. *J. Mater. Chem. A* **2018**, *6*, 17307–17311.
[28] Fan, C. Y.; Wu, H.; Guan, J. Y.; You, X. D.; Yang, C.; Wang, X. Y.; Cao, L.; Shi, B. B.; Peng, Q.; Kong, Y. et al. Scalable fabrication of crystalline COF membranes from amorphous polymeric membranes. *Angew. Chem., Int. Ed.* **2021**, *60*, 18051–18058.
[29] Zhai, Y. F.; Liu, G. Y.; Jin, F. C.; Zhang, Y. Y.; Gong, X. F.; Miao, Z.; Li, J. H.; Zhang, M. Y.; Cui, Y. M.; Zhang, L. Y. et al. Construction of covalent-organic frameworks (COFs) from amorphous covalent organic polymers via linkage replacement. *Angew. Chem., Int. Ed.* **2019**, *58*, 17679–17683.
[30] Miao, Z.; Liu, G. Y.; Cui, Y. M.; Liu, Z. Y.; Li, J. H.; Han, F. W.; Liu, Y.; Sun, X. X.; Gong, X. F.; Zhai, Y. F. et al. A Novel strategy for the construction of covalent organic frameworks from nonporous covalent organic polymers. *Angew. Chem., Int. Ed.* **2019**, *58*, 4906–4910.
[31] Feng, L.; Wang, K. Y.; Joseph, E.; Zhou, H. C. Catalytic porphyrin framework compounds. *Trends Chem.* **2020**, *2*, 555–568.
[32] Liang, Z. Z.; Wang, H. Y.; Zheng, H. Q.; Zhang, W.; Cao, R. Porphyrin-based frameworks for oxygen electrocatalysis and catalytic reduction of carbon dioxide. *Chem. Soc. Rev.* **2021**, *50*, 2540–2581.
[33] Lv, F.; Han, N.; Qiu, Y.; Liu, X. J.; Luo, J.; Li, Y. G. Transition metal macrocycles for heterogeneous electrochemical CO_2 reduction. *Coord. Chem. Rev.* **2020**, *422*, 213435.
[34] Corbin, N.; Zeng, J.; Williams, K.; Manthiram, K. Heterogeneous molecular catalysts for electrocatalytic CO_2 reduction. *Nano Res.* **2019**, *12*, 2093–2125.
[35] Popov, D. A.; Luna, J. M.; Orchanian, N. M.; Haiges, R.; Downes, C. A.; Marinescu, S. C. A 2,2'-bipyridine-containing covalent organic framework bearing rhenium(I) tricarbonyl moieties for CO_2 reduction. *Dalton Trans.* **2018**, *47*, 17450–17460.
[36] Zhao, X. J.; Pachfule, P.; Li, S.; Langenhahn, T.; Ye, M. Y.; Tian, G. Y.; Schmidt, J.; Thomas, A. Silica-templated covalent organic framework-derived Fe-N-doped mesoporous carbon as oxygen reduction electrocatalyst. *Chem. Mater.* **2019**, *31*, 3274–3280.
[37] Zhao, X. J.; Pachfule, P.; Li, S.; Langenhahn, T.; Ye, M. Y.; Schlesiger, C.; Praetz, S.; Schmidt, J.; Thomas, A. Macro/microporous covalent organic frameworks for efficient electrocatalysis. *J. Am. Chem. Soc.* **2019**, *141*, 6623–6630.
[38] Johnson, E. M.; Haiges, R.; Marinescu, S. C. Covalent-organic frameworks composed of rhenium bipyridine and metal porphyrins: Designing heterobimetallic frameworks with two distinct metal sites. *ACS Appl. Mater. Interfaces* **2018**, *10*, 37919–37927.
[39] Wu, D. K.; Xu, Q.; Qian, J.; Li, X. P.; Sun, Y. H. Bimetallic covalent organic frameworks for constructing multifunctional electrocatalyst. *Chem. —Eur. J.* **2019**, *25*, 3105–3111.
[40] Baldwin, L. A.; Crowe, J. W.; Pyles, D. A.; McGrier, P. L. Metalation of a mesoporous three-dimensional covalent organic framework. *J. Am. Chem. Soc.* **2016**, *138*, 15134–15137.
[41] Segura, J. L.; Royuela, S.; Mar Ramos, M. Post-synthetic modification of covalent organic frameworks. *Chem. Soc. Rev.* **2019**, *48*, 3903–3945.
[42] Cusin, L.; Peng, H. J.; Ciesielski, A.; Samori, P. Chemical conversion and locking of the imine linkage: Enhancing the functionality of covalent organic frameworks. *Angew. Chem., Int. Ed.* **2021**, *60*, 14236–14250.
[43] Ding, H. M.; Mal, A.; Wang, C. Tailored covalent organic frameworks by post-synthetic modification. *Mater. Chem. Front.* **2020**, *4*, 113–127.
[44] Feng, X. F.; Gao, Z.; Xiao, L. H.; Lai, Z. Q.; Luo, F. A Ni/Fe complex incorporated into a covalent organic framework as a single-site heterogeneous catalyst for efficient oxygen evolution reaction. *Inorg. Chem. Front.* **2020**, *7*, 3925–3931.
[45] Gao, Z.; Yu, Z. W.; Huang, Y. X.; He, X. Q.; Su, X. M.; Xiao, L. H.; Yu, Y.; Huang, X. H.; Luo, F. Flexible and robust bimetallic covalent organic frameworks for the reversible switching of electrocatalytic oxygen evolution activity. *J. Mater. Chem. A* **2020**, *8*, 5907–5912.
[46] Gao, Z.; Gong, L. L.; He, X. Q.; Su, X. M.; Xiao, L. H.; Luo, F. General strategy to fabricate metal-incorporated pyrolysis-free covalent organic framework for efficient oxygen evolution reaction. *Inorg. Chem.* **2020**, *59*, 4995–5003.
[47] Chen, X.; Huang, N.; Gao, J.; Xu, H.; Xu, F.; Jiang, D. L. Towards covalent organic frameworks with predesignable and aligned open docking sites. *Chem. Commun.* **2014**, *50*, 6161–6163.
[48] Kundu, T.; Wang, J.; Cheng, Y. D.; Du, Y. H.; Qian, Y. H.; Liu, G. L.; Zhao, D. Hydrazone-based covalent organic frameworks for Lewis acid catalysis. *Dalton Trans.* **2018**, *47*, 13824–13829.
[49] Yang, Y. J.; Faheem, M.; Wang, L. L.; Meng, Q. H.; Sha, H. Y.; Yang, N.; Yuan, Y.; Zhu, G. S. Surface pore engineering of covalent organic frameworks for ammonia capture through synergistic multivariate and open metal site approaches. *ACS Cent. Sci.* **2018**, *4*, 748–754.
[50] Ding, S. Y.; Gao, J.; Wang, Q.; Zhang, Y.; Song, W. G.; Su, C. Y.; Wang, W. Construction of covalent organic framework for catalysis: Pd/COF-LZU1 in Suzuki–Miyaura coupling reaction. *J. Am. Chem. Soc.* **2011**, *133*, 19816–19822.
[51] Mu, M. M.; Wang, Y. W.; Qin, Y. T.; Yan, X. L.; Li, Y.; Chen, L. G. Two-dimensional imine-linked covalent organic frameworks as a platform for selective oxidation of olefins. *ACS Appl. Mater. Interfaces* **2017**, *9*, 22856–22863.
[52] Han, X.; Zhang, J.; Huang, J. J.; Wu, X. W.; Yuan, D. Q.; Liu, Y.; Cui, Y. Chiral induction in covalent organic frameworks. *Nat. Commun.* **2018**, *9*, 1294.
[53] Zhang, W. J.; Jiang, P. P.; Wang, Y.; Zhang, J.; Gao, Y. X.; Zhang, P. B. Bottom-up approach to engineer a molybdenum-doped covalent-organic framework catalyst for selective oxidation reaction. *RSC Adv.* **2014**, *4*, 51544–51547.
[54] Li, L. H.; Feng, X. L.; Cui, X. H.; Ma, Y. X.; Ding, S. Y.; Wang, W. Salen-based covalent organic framework. *J. Am. Chem. Soc.* **2017**, *139*, 6042–6045.
[55] Han, X.; Xia, Q. C.; Huang, J. J.; Liu, Y.; Tan, C. X.; Cui, Y. Chiral covalent organic frameworks with high chemical stability for heterogeneous asymmetric catalysis. *J. Am. Chem. Soc.* **2017**, *139*, 8693–8697.
[56] Li, H.; Feng, X.; Shao, P. P.; Chen, J.; Li, C. Z.; Jayakumar, S.; Yang, Q. H. Synthesis of covalent organic frameworks via *in-situ* salen skeleton formation for catalytic applications. *J. Mater. Chem. A* **2019**, *7*, 5482–5492.
[57] Mullangi, D.; Chakraborty, D.; Pradeep, A.; Koshti, V.; Vinod, C. P.; Panja, S.; Nair, S.; Vaidhyanathan, R. Highly stable COF-

supported Co/Co(OH)$_2$ nanoparticles heterogeneous catalyst for reduction of nitrile/nitro compounds under mild conditions. *Small* **2018**, *14*, 1801233.

[58] He, T.; Liu, L.; Wu, G. T.; Chen, P. Covalent triazine framework-supported palladium nanoparticles for catalytic hydrogenation of n-heterocycles. *J. Mater. Chem. A* **2015**, *3*, 16235–16241.

[59] Pachfule, P.; Kandambeth, S.; Díaz Díaz, D.; Banerjee, R. Highly stable covalent organic framework–Au nanoparticles hybrids for enhanced activity for nitrophenol reduction. *Chem. Commun.* **2014**, *50*, 3169–3172.

[60] Lu, S. L.; Hu, Y. M.; Wan, S.; McCaffrey, R.; Jin, Y. H.; Gu, H. W.; Zhang, W. Synthesis of ultrafine and highly dispersed metal nanoparticles confined in a thioether-containing covalent organic framework and their catalytic applications. *J. Am. Chem. Soc.* **2017**, *139*, 17082–17088.

[61] Aijaz, A.; Karkamkar, A.; Choi, Y. J.; Tsumori, N.; Rönnebro, E.; Autrey, T.; Shioyama, H.; Xu, Q. Immobilizing highly catalytically active Pt nanoparticles inside the pores of metal–organic framework: A double solvents approach. *J. Am. Chem. Soc.* **2012**, *134*, 13926–13929.

[62] Liu, H. Y.; Chu, J.; Yin, Z. L.; Cai, X.; Zhuang, L.; Deng, H. X. Covalent organic frameworks linked by amine bonding for concerted electrochemical reduction of CO_2. *Chem* **2018**, *4*, 1696–1709.

[63] Li, L. Y.; Zhao, H. X.; Wang, J. Y.; Wang, R. H. Facile fabrication of ultrafine palladium nanoparticles with size- and location-control in click-based porous organic polymers. *ACS Nano* **2014**, *8*, 5352–5364.

[64] Wang, L.; Nitopi, S. A.; Bertheussen, E.; Orazov, M.; Morales-Guio, C. G.; Liu, X. Y.; Higgins, D. C.; Chan, K.; Nørskov, J. K.; Hahn, C. et al. Electrochemical carbon monoxide reduction on polycrystalline copper: Effects of potential, pressure, and pH on selectivity toward multicarbon and oxygenated products. *ACS Catal.* **2018**, *8*, 7445–7454.

[65] Dinh, C. T.; Burdyny, T.; Kibria, M. G.; Seifitokaldani, A.; Gabardo, C. M.; García de Arquer, F. P.; Kiani, A.; Edwards, J. P.; De Luna, P.; Bushuyev, O. S. et al. CO_2 electroreduction to ethylene via hydroxide-mediated copper catalysis at an abrupt interface. *Science* **2018**, *360*, 783–787.

[66] Huang, J. E.; Li, F. W.; Ozden, A.; Sedighian Rasouli, A.; García de Arquer, F. P.; Liu, S. J.; Zhang, S. Z.; Luo, M. C.; Wang, X.; Lum, Y. et al. CO_2 electrolysis to multicarbon products in strong acid. *Science* **2021**, *372*, 1074–1078.

[67] Côté, A. P.; Benin, A. I.; Ockwig, N. W.; Keeffe, M.; Matzger, A. J.; Yaghi, O. M. Porous, crystalline, covalent organic frameworks. *Science* **2005**, *310*, 1166.

[68] Campbell, N. L.; Clowes, R.; Ritchie, L. K.; Cooper, A. I. Rapid microwave synthesis and purification of porous covalent organic frameworks. *Chem. Mater.* **2009**, *21*, 204–206.

[69] Zhu, Y. L.; Wan, S.; Jin, Y. H.; Zhang, W. Desymmetrized vertex design for the synthesis of covalent organic frameworks with periodically heterogeneous pore structures. *J. Am. Chem. Soc.* **2015**, *137*, 13772–13775.

[70] Wei, H.; Chai, S. Z.; Hu, N. T.; Yang, Z.; Wei, L. M.; Wang, L. The microwave-assisted solvothermal synthesis of a crystalline two-dimensional covalent organic framework with high CO_2 capacity. *Chem. Commun.* **2015**, *51*, 12178–12181.

[71] Lee, G. Y.; Lee, J.; Vo, H. T.; Kim, S.; Lee, H.; Park, T. Amine-functionalized covalent organic framework for efficient SO_2 capture with high reversibility. *Sci. Rep.* **2017**, *7*, 557.

[72] Biswal, B. P.; Chandra, S.; Kandambeth, S.; Lukose, B.; Heine, T.; Banerjee, R. Mechanochemical synthesis of chemically stable isoreticular covalent organic frameworks. *J. Am. Chem. Soc.* **2013**, *135*, 5328–5331.

[73] Das, G.; Balaji Shinde, D.; Kandambeth, S.; Biswal, B. P.; Banerjee, R. Mechanosynthesis of imine, β-ketoenamine, and hydrogen-bonded imine-linked covalent organic frameworks using liquid-assisted grinding. *Chem. Commun.* **2014**, *50*, 12615–12618.

[74] Shinde, D. B.; Aiyappa, H. B.; Bhadra, M.; Biswal, B. P.; Wadge, P.; Kandambeth, S.; Garai, B.; Kundu, T.; Kurungot, S.; Banerjee, R. A mechanochemically synthesized covalent organic framework as a proton-conducting solid electrolyte. *J. Mater. Chem. A* **2016**, *4*, 2682–2690.

[75] Yang, S. T.; Kim, J.; Cho, H. Y.; Kim, S.; Ahn, W. S. Facile synthesis of covalent organic frameworks COF-1 and COF-5 by sonochemical method. *RSC Adv.* **2012**, *2*, 10179–10181.

[76] Jiang, Y.; Huang, W.; Wang, J. Y.; Wu, Q.; Wang, H. J.; Pan, L. F.; Liu, X. K. Green, scalable and morphology controlled synthesis of nanofibrous covalent organic frameworks and their nanohybrids through a vapor-assisted solid-state approach. *J. Mater. Chem. A* **2014**, *2*, 8201–8204.

[77] Medina, D. D.; Rotter, J. M.; Hu, Y. H.; Dogru, M.; Werner, V.; Auras, F.; Markiewicz, J. T.; Knochel, P.; Bein, T. Room temperature synthesis of covalent-organic framework films through vapor-assisted conversion. *J. Am. Chem. Soc.* **2015**, *137*, 1016–1019.

[78] Smith, B. J.; Dichtel, W. R. Mechanistic studies of two-dimensional covalent organic frameworks rapidly polymerized from initially homogenous conditions. *J. Am. Chem. Soc.* **2014**, *136*, 8783–8789.

[79] Smith, B. J.; Hwang, N.; Chavez, A. D.; Novotney, J. L.; Dichtel, W. R. Growth rates and water stability of 2D boronate ester covalent organic frameworks. *Chem. Commun.* **2015**, *51*, 7532–7535.

[80] Koo, B. T.; Heden, R. F.; Clancy, P. Nucleation and growth of 2D covalent organic frameworks: Polymerization and crystallization of COF monomers. *Phys. Chem. Chem. Phys.* **2017**, *19*, 9745–9754.

[81] Li, H. Y.; Chavez, A. D.; Li, H. F.; Li, H.; Dichtel, W. R.; Bredas, J. L. Nucleation and growth of covalent organic frameworks from solution: The example of COF-5. *J. Am. Chem. Soc.* **2017**, *139*, 16310–16318.

[82] Nguyen, V.; Grünwald, M. Microscopic origins of poor crystallinity in the synthesis of covalent organic framework COF-5. *J. Am. Chem. Soc.* **2018**, *140*, 3306–3311.

[83] Li, H. Y.; Evans, A. M.; Castano, I.; Strauss, M. J.; Dichtel, W. R.; Bredas, J. L. Nucleation-elongation dynamics of two-dimensional covalent organic frameworks. *J. Am. Chem. Soc.* **2020**, *142*, 1367–1374.

[84] Ciaccia, M.; Di Stefano, S. Mechanisms of imine exchange reactions in organic solvents. *Org. Biomol. Chem.* **2015**, *13*, 646–654.

[85] Gao, Q.; Bai, L. Y.; Zeng, Y. F.; Wang, P.; Zhang, X. J.; Zou, R. Q.; Zhao, Y. L. Reconstruction of covalent organic frameworks by dynamic equilibrium. *Chem.—Eur. J.* **2015**, *21*, 16818–16822.

[86] Smith, B. J.; Overholts, A. C.; Hwang, N.; Dichtel, W. R. Insight into the crystallization of amorphous imine-linked polymer networks to 2D covalent organic frameworks. *Chem. Commun.* **2016**, *52*, 3690–3693.

[87] Wang, H.; He, B.; Liu, F.; Stevens, C.; Brady, M. A.; Cai, S.; Wang, C.; Russell, T. P.; Tan, T. W.; Liu, Y. Orientation transitions during the growth of imine covalent organic framework thin films. *J. Mater. Chem. C* **2017**, *5*, 5090–5095.

[88] Feriante, C.; Evans, A. M.; Jhulki, S.; Castano, I.; Strauss, M. J.; Barlow, S.; Dichtel, W. R.; Marder, S. R. New mechanistic insights into the formation of imine-linked two-dimensional covalent organic frameworks. *J. Am. Chem. Soc.* **2020**, *142*, 18637–18644.

[89] Jiang, D. L. Covalent organic frameworks: An amazing chemistry platform for designing polymers. *Chem* **2020**, *6*, 2461–2483.

[90] Kuhn, P.; Antonietti, M.; Thomas, A. Porous, covalent triazine-based frameworks prepared by ionothermal synthesis. *Angew. Chem., Int. Ed.* **2008**, *47*, 3450–3453.

[91] Jackson, K. T.; Reich, T. E.; El-Kaderi, H. M. Targeted synthesis of a porous borazine-linked covalent organic framework. *Chem. Commun.* **2012**, *48*, 8823–8825.

[92] Wang, K. W.; Yang, L. M.; Wang, X.; Guo, L. P.; Cheng, G.; Zhang, C.; Jin, S. B.; Tan, B. E.; Cooper, A. Covalent triazine frameworks via a low-temperature polycondensation approach. *Angew. Chem., Int. Ed.* **2017**, *56*, 14149–14153.

[93] Liu, M. Y.; Huang, Q.; Wang, S. L.; Li, Z. Y.; Li, B. Y.; Jin, S. B.; Tan, B. E. Crystalline covalent triazine frameworks by *in-situ* oxidation of alcohols to aldehyde monomers. *Angew. Chem., Int. Ed.* **2018**, *57*, 11968–11972.

[94] Jiang, S. Y.; Gan, S. X.; Zhang, X.; Li, H.; Qi, Q. Y.; Cui, F. Z.;

Lu, J.; Zhao, X. Aminal-linked covalent organic frameworks through condensation of secondary amine with aldehyde. *J. Am. Chem. Soc.* **2019**, *141*, 14981–14986.

[95] Uribe-Romo, F. J.; Doonan, C. J.; Furukawa, H.; Oisaki, K.; Yaghi, O. M. Crystalline covalent organic frameworks with hydrazone linkages. *J. Am. Chem. Soc.* **2011**, *133*, 11478–11481.

[96] DeBlase, C. R.; Silberstein, K. E.; Truong, T. T.; Abruña, H. D.; Dichtel, W. R. β-Ketoenamine-linked covalent organic frameworks capable of pseudocapacitive energy storage. J. Am. *Chem. Soc.* **2013**, *135*, 16821–16824.

[97] Dalapati, S.; Jin, S. B.; Gao, J.; Xu, Y. H.; Nagai, A.; Jiang, D. L. An azine-linked covalent organic framework. *J. Am. Chem. Soc.* **2013**, *135*, 17310–17313.

[98] Nagai, A.; Chen, X.; Feng, X.; Ding, X. S.; Guo, Z. Q.; Jiang, D. L. A squaraine-linked mesoporous covalent organic framework. *Angew. Chem., Int. Ed.* **2013**, *52*, 3770–3774.

[99] Das, G.; Biswal, B. P.; Kandambeth, S.; Venkatesh, V.; Kaur, G.; Addicoat, M.; Heine, T.; Verma, S.; Banerjee, R. Chemical sensing in two dimensional porous covalent organic nanosheets. *Chem. Sci.* **2015**, *6*, 3931–3939.

[100] Li, X.; Wang, H.; Chen, Z. X.; Xu, H. S.; Yu, W.; Liu, C. B.; Wang, X. W.; Zhang, K.; Xie, K. Y.; Loh, K. P. Covalent-organic-framework-based Li-CO_2 batteries. *Adv. Mater.* **2019**, *31*, 1905879.

[101] Li, Z. P.; Feng, X.; Zou, Y. C.; Zhang, Y. W.; Xia, H.; Liu, X. M.; Mu, Y. A 2D azine-linked covalent organic framework for gas storage applications. *Chem. Commun.* **2014**, *50*, 13825–13828.

[102] Li, Z. P.; Zhang, Y. W.; Xia, H.; Mu, Y.; Liu, X. M. A robust and luminescent covalent organic framework as a highly sensitive and selective sensor for the detection of Cu^{2+} ions. *Chem. Commun.* **2016**, *52*, 6613–6616.

[103] Qian, C.; Zhou, W. Q.; Qiao, J. S.; Wang, D. D.; Li, X.; Teo, W. L.; Shi, X. Y.; Wu, H. W.; Di, J.; Wang, H. et al. Linkage engineering by harnessing supramolecular interactions to fabricate 2D hydrazone-linked covalent organic framework platforms toward advanced catalysis. *J. Am. Chem. Soc.* **2020**, *142*, 18138–18149.

[104] Li, Z. P.; Geng, K. Y.; He, T.; Tan, K. T.; Huang, N.; Jiang, Q. H.; Nagao, Y.; Jiang, D. L. Editing light emission with stable crystalline covalent organic frameworks via wall surface perturbation. *Angew. Chem., Int. Ed.* **2021**, *60*, 19419–19427.

[105] Li, Z. P.; Huang, N.; Lee, K. H.; Feng, Y.; Tao, S. S.; Jiang, Q. H.; Nagao, Y.; Irle, S.; Jiang, D. L. Light-emitting covalent organic frameworks: Fluorescence improving via pinpoint surgery and selective switch-on sensing of anions. *J. Am. Chem. Soc.* **2018**, *140*, 12374–12377.

[106] Liang, R. R.; A, R. H.; Xu, S. Q.; Qi, Q. Y.; Zhao, X. Fabricating organic nanotubes through selective disassembly of two-dimensional covalent organic frameworks. *J. Am. Chem. Soc.* **2020**, *142*, 70–74.

[107] Halder, A.; Ghosh, M.; Khayum M, A.; Bera, S.; Addicoat, M.; Sasmal, H. S.; Karak, S.; Kurungot, S.; Banerjee, R. Interlayer hydrogen-bonded covalent organic frameworks as high-performance supercapacitors. *J. Am. Chem. Soc.* **2018**, *140*, 10941–10945.

[108] Khayum M, A.; Vijayakumar, V.; Karak, S.; Kandambeth, S.; Bhadra, M.; Suresh, K.; Acharambath, N.; Kurungot, S.; Banerjee, R. Convergent covalent organic framework thin sheets as flexible supercapacitor electrodes. *ACS Appl. Mater. Interfaces* **2018**, *10*, 28139–28146.

[109] Rao, M. R.; Fang, Y.; De Feyter, S.; Perepichka, D. F. Conjugated covalent organic frameworks via Michael addition-elimination. *J. Am. Chem. Soc.* **2017**, *139*, 2421–2427.

[110] Zhao, C. F.; Diercks, C. S.; Zhu, C. H.; Hanikel, N.; Pei, X. K.; Yaghi, O. M. Urea-linked covalent organic frameworks. *J. Am. Chem. Soc.* **2018**, *140*, 16438–16441.

[111] Waller, P. J.; AlFaraj, Y. S.; Diercks, C. S.; Jarenwattananon, N. N.; Yaghi, O. M. Conversion of imine to oxazole and thiazole linkages in covalent organic frameworks. *J. Am. Chem. Soc.* **2018**, *140*, 9099–9103.

[112] Das, P.; Mandal, S. K. In-depth experimental and computational investigations for remarkable gas/vapor sorption, selectivity, and affinity by a porous nitrogen-rich covalent organic framework. *Chem. Mater.* **2019**, *31*, 1584–1596.

[113] Guo, J.; Xu, Y. H.; Jin, S. B.; Chen, L.; Kaji, T.; Honsho, Y.; Addicoat, M. A.; Kim, J.; Saeki, A.; Ihee, H. et al. Conjugated organic framework with three-dimensionally ordered stable structure and delocalized π clouds. *Nat. Commun.* **2013**, *4*, 2736.

[114] Liu, J.; Yang, T.; Wang, Z. P.; Wang, P. L.; Feng, J.; Ding, S. Y.; Wang, W. Pyrimidazole-based covalent organic frameworks: Integrating functionality and ultrastability via isocyanide chemistry. *J. Am. Chem. Soc.* **2020**, *142*, 20956–20961.

[115] Fang, Q. R.; Zhuang, Z. B.; Gu, S.; Kaspar, R. B.; Zheng, J.; Wang, J. H.; Qiu, S. L.; Yan, Y. S. Designed synthesis of large-pore crystalline polyimide covalent organic frameworks. *Nat. Commun.* **2014**, *5*, 4503.

[116] Jin, E. Q.; Asada, M.; Xu, Q.; Dalapati, S.; Addicoat, M. A.; Brady, M. A.; Xu, H.; Nakamura, T.; Heine, T.; Chen, Q. H. et al. Two-dimensional sp^2 carbon-conjugated covalent organic frameworks. *Science* **2017**, *357*, 673–676.

[117] Lyu, H.; Diercks, C. S.; Zhu, C. H.; Yaghi, O. M. Porous crystalline olefin-linked covalent organic frameworks. *J. Am. Chem. Soc.* **2019**, *141*, 6848–6852.

[118] Waller, P. J.; Lyle, S. J.; Osborn Popp, T. M.; Diercks, C. S.; Reimer, J. A.; Yaghi, O. M. Chemical conversion of linkages in covalent organic frameworks. *J. Am. Chem. Soc.* **2016**, *138*, 15519–15522.

[119] Das, G.; Skorjanc, T.; Sharma, S. K.; Gándara, F.; Lusi, M.; Shankar Rao, D. S.; Vimala, S.; Krishna Prasad, S.; Raya, J.; Han, D. S. et al. Viologen-based conjugated covalent organic networks via Zincke reaction. *J. Am. Chem. Soc.* **2017**, *139*, 9558–9565.

[120] Zhang, B.; Wei, M. F.; Mao, H. Y.; Pei, X. K.; Alshmimri, S. A.; Reimer, J. A.; Yaghi, O. M. Crystalline dioxin-linked covalent organic frameworks from irreversible reactions. *J. Am. Chem. Soc.* **2018**, *140*, 12715–12719.

[121] Zhao, C. F.; Lyu, H.; Ji, Z.; Zhu, C. H.; Yaghi, O. M. Ester-linked crystalline covalent organic frameworks. *J. Am. Chem. Soc.* **2020**, *142*, 14450–14454.

[122] Liu, S. S.; Wang, M. F.; Qian, T.; Ji, H. Q.; Liu, J.; Yan, C. L. Facilitating nitrogen accessibility to boron-rich covalent organic frameworks via electrochemical excitation for efficient nitrogen fixation. *Nat. Commun.* **2019**, *10*, 3898.

[123] Ma, L. S.; Hu, W. B.; Mei, B. B.; Liu, H.; Yuan, B.; Zang, J.; Chen, T.; Zou, L. L.; Zou, Z. Q.; Yang, B. et al. Covalent triazine framework confined copper catalysts for selective electrochemical CO_2 reduction: Operando diagnosis of active sites. *ACS Catal.* **2020**, *10*, 4534–4542.

[124] Lu, C. B.; Yang, J.; Wei, S. C.; Bi, S.; Xia, Y.; Chen, M. X.; Hou, Y.; Qiu, M.; Yuan, C.; Su, Y. Z. et al. Atomic Ni anchored covalent triazine framework as high efficient electrocatalyst for carbon dioxide conversion. *Adv. Funct. Mater.* **2019**, *29*, 1806884.

[125] Zuo, Q.; Zhao, P. P.; Luo, W.; Cheng, G. Z. Hierarchically porous Fe–N–C derived from covalent-organic materials as a highly efficient electrocatalyst for oxygen reduction. *Nanoscale* **2016**, *8*, 14271–14277.

[126] Lin, S.; Diercks, C. S.; Zhang, Y. B.; Kornienko, N.; Nichols, E. M.; Zhao, Y. B.; Paris, A. R.; Kim, D.; Yang, P. D.; Yaghi, O. M. et al. Covalent organic frameworks comprising cobalt porphyrins for catalytic CO_2 reduction in water. *Science* **2015**, *349*, 1208.

[127] Diercks, C. S.; Lin, S.; Kornienko, N.; Kapustin, E. A.; Nichols, E. M.; Zhu, C. H.; Zhao, Y. B.; Chang, C. J.; Yaghi, O. M. Reticular electronic tuning of porphyrin active sites in covalent organic frameworks for electrocatalytic carbon dioxide reduction. *J. Am. Chem. Soc.* **2018**, *140*, 1116–1122.

[128] Sun, S. W.; Wang, G. F.; Zhou, Y.; Wang, F. B.; Xia, X. H. High-performance Ru@C_4N electrocatalyst for hydrogen evolution reaction in both acidic and alkaline solutions. *ACS Appl. Mater. Interfaces* **2019**, *11*, 19176–19182.

[129] Huang, N.; Lee, K. H.; Yue, Y.; Xu, X. Y.; Irle, S.; Jiang, Q. H.; Jiang, D. L. A stable and conductive metallophthalocyanine framework for electrocatalytic carbon dioxide reduction in water. *Angew. Chem., Int. Ed.* **2020**, *59*, 16587–16593.

[130] Zhang, M. D.; Si, D. H.; Yi, J. D.; Zhao, S. S.; Huang, Y. B.; Cao, R. Conductive phthalocyanine-based covalent organic framework

for highly efficient electroreduction of carbon dioxide. *Small* **2020**, *16*, 2005254.

[131] Chandran Ranjeesh, K.; Illathvalappil, R.; Chandrakant Wakchaure, V.; Goudappagouda; Kurungot, S.; Babu, S. S. Metalloporphyrin two-dimensional polymers via metal-catalyst-free C–C bond formation for efficient catalytic hydrogen evolution. *ACS Appl. Energy Mater.* **2018**, *1*, 6442–6450.

[132] Zhai, L. P.; Yang, S.; Yang, X. B.; Ye, W. Y.; Wang, J.; Chen, W. H.; Guo, Y.; Mi, L. W.; Wu, Z. J.; Soutis, C. et al. Conjugated covalent organic frameworks as platinum nanoparticle supports for catalyzing the oxygen reduction reaction. *Chem. Mater.* **2020**, *32*, 9747–9752.

[133] Royuela, S.; Martínez-Periñán, E.; Arrieta, M. P.; Martínez, J. I.; Ramos, M. M.; Zamora, F.; Lorenzo, E.; Segura, J. L. Oxygen reduction using a metal-free naphthalene diimide-based covalent organic framework electrocatalyst. *Chem. Commun.* **2020**, *56*, 1267–1270.

[134] Lu, M.; Zhang, M.; Liu, C. G.; Liu, J.; Shang, L. J.; Wang, M.; Chang, J. N.; Li, S. L.; Lan, Y. Q. Stable dioxin-linked metallophthalocyanine covalent organic frameworks (COFs) as photo-coupled electrocatalysts for CO_2 reduction. *Angew. Chem., Int. Ed.* **2021**, *60*, 4864–4871.

[135] Tavakoli, E.; Kakekhani, A.; Kaviani, S.; Tan, P.; Ghaleni, M. M.; Zaeem, M. A.; Rappe, A. M.; Nejati, S. *In-situ* bottom-up synthesis of porphyrin-based covalent organic frameworks. *J. Am. Chem. Soc.* **2019**, *141*, 19560–19564.

[136] Zhu, D. Y.; Li, X. Y.; Li, Y. L.; Barnes, M.; Tseng, C. P.; Khalil, S.; Rahman, M. M.; Ajayan, P. M.; Verduzco, R. Transformation of one-dimensional linear polymers into two-dimensional covalent organic frameworks through sequential reversible and irreversible chemistries. *Chem. Mater.* **2021**, *33*, 413–419.

[137] Zhang, G.; Tsujimoto, M.; Packwood, D.; Duong, N. T.; Nishiyama, Y.; Kadota, K.; Kitagawa, S.; Horike, S. Construction of a hierarchical architecture of covalent organic frameworks via a postsynthetic approach. *J. Am. Chem. Soc.* **2018**, *140*, 2602–2609.

[138] Qian, C.; Qi, Q. Y.; Jiang, G. F.; Cui, F. Z.; Tian, Y.; Zhao, X. Toward covalent organic frameworks bearing three different kinds of pores: The strategy for construction and COF-to-COF transformation via heterogeneous linker exchange. *J. Am. Chem. Soc.* **2017**, *139*, 6736–6743.

[139] Shan, Z.; Wu, X. W.; Xu, B. Q.; Hong, Y. L.; Wu, M. M.; Wang, Y. X.; Nishiyama, Y.; Zhu, J. W.; Horike, S.; Kitagawa, S. et al. Dynamic transformation between covalent organic frameworks and discrete organic cages. *J. Am. Chem. Soc.* **2020**, *142*, 21279–21284.

[140] Daugherty, M. C.; Vitaku, E.; Li, R. L.; Evans, A. M.; Chavez, A. D.; Dichtel, W. R. Improved synthesis of β-ketoenamine-linked covalent organic frameworks via monomer exchange reactions. *Chem. Commun.* **2019**, *55*, 2680–2683.

[141] Qian, H. L.; Meng, F. L.; Yang, C. X.; Yan, X. P. Irreversible amide-linked covalent organic framework for selective and ultrafast gold recovery. *Angew. Chem., Int. Ed.* **2020**, *59*, 17607–17613.

[142] Li, Z.; Ding, X. S.; Feng, Y. Y.; Feng, W.; Han, B. H. Structural and dimensional transformations between covalent organic frameworks via linker exchange. *Macromolecules* **2019**, *52*, 1257–1265.

[143] Cao, C. L.; Wang, H. J.; Wang, M. D.; Liu, Y.; Zhang, Z. M.; Liang, S. W.; Yuhan, W.; Pan, F. S.; Jiang, Z. Y. Conferring efficient alcohol dehydration to covalent organic framework membranes via post-synthetic linker exchange. *J. Membr. Sci.* **2021**, *630*, 119319.

[144] Guan, C. Z.; Wang, D.; Wan, L. J. Construction and repair of highly ordered 2D covalent networks by chemical equilibrium regulation. *Chem. Commun.* **2012**, *48*, 2943–2945.

[145] Stewart, D.; Antypov, D.; Dyer, M. S.; Pitcher, M. J.; Katsoulidis, A. P.; Chater, P. A.; Blanc, F.; Rosseinsky, M. J. Stable and ordered amide frameworks synthesised under reversible conditions which facilitate error checking. *Nat. Commun.* **2017**, *8*, 1102.

[146] Matsumoto, M.; Dasari, R. R.; Ji, W.; Feriante, C. H.; Parker, T. C.; Marder, S. R.; Dichtel, W. R. Rapid, low temperature formation of imine-linked covalent organic frameworks catalyzed by metal triflates. *J. Am. Chem. Soc.* **2017**, *139*, 4999–5002.

[147] Guan, X. Y.; Ma, Y. C.; Li, H.; Yusran, Y.; Xue, M.; Fang, Q. R.; Yan, Y. S.; Valtchev, V.; Qiu, S. L. Fast, ambient temperature and pressure ionothermal synthesis of three-dimensional covalent organic frameworks. *J. Am. Chem. Soc.* **2018**, *140*, 4494–4498.

[148] Tan, J.; Namuangruk, S.; Kong, W. F.; Kungwan, N.; Guo, J.; Wang, C. C. Manipulation of amorphous-to-crystalline transformation: Towards the construction of covalent organic framework hybrid microspheres with NIR photothermal conversion ability. *Angew. Chem., Int. Ed.* **2016**, *55*, 13979–13984.

[149] Karak, S.; Kumar, S.; Pachfule, P.; Banerjee, R. Porosity prediction through hydrogen bonding in covalent organic frameworks. *J. Am. Chem. Soc.* **2018**, *140*, 5138–5145.

[150] Matsumoto, M.; Valentino, L.; Stiehl, G. M.; Balch, H. B.; Corcos, A. R.; Wang, F.; Ralph, D. C.; Mariñas, B. J.; Dichtel, W. R. Lewis-acid-catalyzed interfacial polymerization of covalent organic framework films. *Chem* **2018**, *4*, 308–317.

[151] Gao, Y. N.; Wang, C.; Hu, H.; Ge, R. L.; Lu, M. H.; Zhang, J. Q.; Li, Z. P.; Shao, P. P.; Jiang, D. L. Synthesis of two-dimensional covalent organic frameworks in ionic liquids. *Chem.—Eur. J.* **2019**, *25*, 15488–15492.

[152] Antonietti, M.; Kuang, D. B.; Smarsly, B.; Zhou, Y. Ionic liquids for the convenient synthesis of functional nanoparticles and other inorganic nanostructures. *Angew. Chem., Int. Ed.* **2004**, *43*, 4988–4992.

[153] Qiu, J. K.; Wang, H. Y.; Zhao, Y. L.; Guan, P. X.; Li, Z. Y.; Zhang, H. C.; Gao, H. S.; Zhang, S. J.; Wang, J. J. Hierarchically porous covalent organic frameworks assembled in ionic liquids for highly effective catalysis of C–C coupling reactions. *Green Chem.* **2020**, *22*, 2605–2612.

[154] Guan, P. X.; Qiu, J. K.; Zhao, Y. L.; Wang, H. Y.; Li, Z. Y.; Shi, Y. L.; Wang, J. J. A novel crystalline azine-linked three-dimensional covalent organic framework for CO_2 capture and conversion. *Chem. Commun.* **2019**, *55*, 12459–12462.

[155] Zhao, L. M.; Liu, H. M.; Du, Y.; Liang, X.; Wang, W. J.; Zhao, H.; Li, W. Z. An ionic liquid as a green solvent for high potency synthesis of 2D covalent organic frameworks. *New J. Chem.* **2020**, *44*, 15410–15414.

[156] Dong, B.; Wang, W. J.; Pan, W.; Kang, G. J. Ionic liquid as a green solvent for ionothermal synthesis of 2D keto-enamine-linked covalent organic frameworks. *Mater. Chem. Phys.* **2019**, *226*, 244–249.

[157] Gao, S. Q.; Li, Z. Y.; Yang, Y. Y.; Wang, Z. Z.; Wang, Y. L.; Luo, S. J.; Yao, K. S.; Qiu, J. K.; Wang, H. Y.; Cao, L. et al. The ionic liquid–H_2O interface: A new platform for the synthesis of highly crystalline and molecular sieving covalent organic framework membranes. *ACS Appl. Mater. Interfaces* **2021**, *13*, 36507–36516.

[158] Calik, M.; Sick, T.; Dogru, M.; Döblinger, M.; Datz, S.; Budde, H.; Hartschuh, A.; Auras, F.; Bein, T. From highly crystalline to outer surface-functionalized covalent organic frameworks-a modulation approach. *J. Am. Chem. Soc.* **2016**, *138*, 1234–1239.

[159] Castano, I.; Evans, A. M.; Li, H. Y.; Vitaku, E.; Strauss, M. J.; Brédas, J. L.; Gianneschi, N. C.; Dichtel, W. R. Chemical control over nucleation and anisotropic growth of two-dimensional covalent organic frameworks. *ACS Cent. Sci.* **2019**, *5*, 1892–1899.

[160] Zhao, W.; Wang, T. P.; Wu, J. L.; Pan, R. P.; Liu, X. Y.; Liu, X. K. Monolithic covalent organic framework aerogels through framework crystallization induced self-assembly: Heading towards framework materials synthesis over all length scales. *Chin. J. Polym. Sci.* **2019**, *37*, 1045–1052.

[161] Wang, S.; Zhang, Z. Y.; Zhang, H. M.; Rajan, A. G.; Xu, N.; Yang, Y. H.; Zeng, Y. W.; Liu, P. W.; Zhang, X. H.; Mao, Q. Y. et al. Reversible polycondensation-termination growth of covalent-organic-framework spheres, fibers, and films. *Matter* **2019**, *1*, 1592–1605.

[162] Chen, X. S.; Xia, L. Y.; Pan, R. P.; Liu, X. K. Covalent organic framework mesocrystals through dynamic modulator manipulated mesoscale self-assembly of imine macrocycle precursors. *J. Colloid Interface Sci.* **2020**, *568*, 76–80.

[163] Ma, T. Q.; Kapustin, E. A.; Yin, S. X.; Liang, L.; Zhou, Z. Y.; Niu, J.; Li, L. H.; Wang, Y. Y.; Su, J.; Li, J. et al. Single-crystal X-ray diffraction structures of covalent organic frameworks. *Science*

2018, *361*, 48–52.
[164] Liang, L.; Qiu, Y.; Wang, W. D.; Han, J.; Luo, Y.; Yu, W.; Yin, G. L.; Wang, Z. P.; Zhang, L.; Ni, J. W. et al. Non-interpenetrated single-crystal covalent organic frameworks. *Angew. Chem., Int. Ed.* **2020**, *59*, 17991–17995.
[165] Maia, R. A.; Oliveira, F. L.; Nazarkovsky, M.; Esteves, P. M. Crystal engineering of covalent organic frameworks based on hydrazine and hydroxy-1,3,5-triformylbenzenes. *Cryst. Growth Des.* **2018**, *18*, 5682–5689.
[166] Zhu, D. Y.; Alemany, L. B.; Guo, W. H.; Verduzco, R. Enhancement of crystallinity of imine-linked covalent organic frameworks via aldehyde modulators. *Polym. Chem.* **2020**, *11*, 4464–4468.
[167] Zhao, W.; Qiao, J.; Ning, T. L.; Liu, X. K. Scalable ambient pressure synthesis of covalent organic frameworks and their colorimetric nanocomposites through dynamic imine exchange reactions. *Chin. J. Polym. Sci.* **2018**, *36*, 1–7.
[168] Liu, K. J.; Qi, H. Y.; Dong, R. H.; Shivhare, R.; Addicoat, M.; Zhang, T.; Sahabudeen, H.; Heine, T.; Mannsfeld, S.; Kaiser, U. et al. On-water surface synthesis of crystalline, few-layer two-dimensional polymers assisted by surfactant monolayers. *Nat. Chem.* **2019**, *11*, 994–1000.
[169] Sahabudeen, H.; Qi, H. Y.; Ballabio, M.; Položij, M.; Olthof, S.; Shivhare, R.; Jing, Y.; Park, S.; Liu, K. J.; Zhang, T. et al. Highly crystalline and semiconducting imine-based two-dimensional polymers enabled by interfacial synthesis. *Angew. Chem., Int. Ed.* **2020**, *59*, 6028–6036.
[170] Park, S.; Liao, Z. Q.; Ibarlucea, B.; Qi, H. Y.; Lin, H. H.; Becker, D.; Melidonie, J.; Zhang, T.; Sahabudeen, H.; Baraban, L. et al. Two-dimensional boronate ester covalent organic framework thin films with large single crystalline domains for a neuromorphic memory device. *Angew. Chem., Int. Ed.* **2020**, *59*, 8218–8224.
[171] Chen, Y. C.; Shi, Z. L.; Wei, L.; Zhou, B. B.; Tan, J.; Zhou, H. L.; Zhang, Y. B. Guest-dependent dynamics in a 3D covalent organic framework. *J. Am. Chem. Soc.* **2019**, *141*, 3298–3303.
[172] Hao, Q.; Zhao, C. Q.; Sun, B.; Lu, C.; Liu, J.; Liu, M. J.; Wan, L. J.; Wang, D. Confined synthesis of two-dimensional covalent organic framework thin films within superspreading water layer. *J. Am. Chem. Soc.* **2018**, *140*, 12152–12158.
[173] Sasmal, H. S.; Halder, A.; Kunjattu H, S.; Dey, K.; Nadol, A.; Ajithkumar, T. G.; Ravindra Bedadur, P.; Banerjee, R. Covalent self-assembly in two dimensions: Connecting covalent organic framework nanospheres into crystalline and porous thin films. *J. Am. Chem. Soc.* **2019**, *141*, 20371–20379.
[174] Liu, M. Y.; Jiang, K.; Ding, X.; Wang, S. L.; Zhang, C. X.; Liu, J.; Zhan, Z.; Cheng, G.; Li, B. Y.; Chen, H. et al. Controlling monomer feeding rate to achieve highly crystalline covalent triazine frameworks. *Adv. Mater.* **2019**, *31*, 1807865.
[175] Li, R. L.; Flanders, N. C.; Evans, A. M.; Ji, W.; Castano, I.; Chen, L. X.; Gianneschi, N. C.; Dichtel, W. R. Controlled growth of imine-linked two-dimensional covalent organic framework nanoparticles. *Chem. Sci.* **2019**, *10*, 3796–3801.
[176] Evans, A. M.; Parent, L. R.; Flanders, N. C.; Bisbey, R. P.; Vitaku, E.; Kirschner, M. S.; Schaller, R. D.; Chen, L. X.; Gianneschi, N. C.; Dichtel, W. R. Seeded growth of single-crystal two-dimensional covalent organic frameworks. *Science* **2018**, *361*, 52–57.
[177] Vitaku, E.; Dichtel, W. R. Synthesis of 2D imine-linked covalent organic frameworks through formal transimination reactions. *J. Am. Chem. Soc.* **2017**, *139*, 12911–12914.
[178] Liu, Y. Z.; Wang, Y. J.; Li, H.; Guan, X. Y.; Zhu, L. K.; Xue, M.; Yan, Y. S.; Valtchev, V.; Qiu, S. L.; Fang, Q. R. Ambient aqueous-phase synthesis of covalent organic frameworks for degradation of organic pollutants. *Chem. Sci.* **2019**, *10*, 10815–10820.
[179] Zhao, Y. B.; Guo, L.; Gándara, F.; Ma, Y. H.; Liu, Z.; Zhu, C. H.; Lyu, H.; Trickett, C. A.; Kapustin, E. A.; Terasaki, O. et al. A synthetic route for crystals of woven structures, uniform nanocrystals, and thin films of imine covalent organic frameworks. *J. Am. Chem. Soc.* **2017**, *139*, 13166–13172.
[180] Li, Z. J.; Ding, S. Y.; Xue, H. D.; Cao, W.; Wang, W. Synthesis of –C=N– linked covalent organic frameworks via the direct condensation of acetals and amines. *Chem. Commun.* **2016**, *52*, 7217–7220.
[181] Spitler, E. L.; Giovino, M. R.; White, S. L.; Dichtel, W. R. A mechanistic study of Lewis acid-catalyzed covalent organic framework formation. *Chem. Sci.* **2011**, *2*, 1588–1593.
[182] Spitler, E. L.; Dichtel, W. R. Lewis acid-catalysed formation of two-dimensional phthalocyanine covalent organic frameworks. *Nat. Chem.* **2010**, *2*, 672–677.
[183] Dogru, M.; Sonnauer, A.; Zimdars, S.; Döblinger, M.; Knochel, P.; Bein, T. Facile synthesis of a mesoporous benzothiadiazole-COF based on a transesterification process. *CrystEngComm* **2013**, *15*, 1500–1502.
[184] Zhu, H. J.; Lu, M.; Wang, Y. R.; Yao, S. J.; Zhang, M.; Kan, Y. H.; Liu, J.; Chen, Y. F.; Li, S. L.; Lan, Y. Q. Efficient electron transmission in covalent organic framework nanosheets for highly active electrocatalytic carbon dioxide reduction. *Nat. Commun.* **2020**, *11*, 497.
[185] Berlanga, I.; Ruiz-González, M. L.; González-Calbet, J. M.; Fierro, J. L. G.; Mas-Ballesté, R.; Zamora, F. Delamination of layered covalent organic frameworks. *Small* **2011**, *7*, 1207–1211.
[186] Berlanga, I.; Mas-Ballesté, R.; Zamora, F. Tuning delamination of layered covalent organic frameworks through structural design. *Chem. Commun.* **2012**, *48*, 7976–7978.
[187] Li, G.; Zhang, K.; Tsuru, T. Two-dimensional covalent organic framework (COF) membranes fabricated via the assembly of exfoliated cof nanosheets. *ACS Appl. Mater. Interfaces* **2017**, *9*, 8433–8436.
[188] Bunck, D. N.; Dichtel, W. R. Bulk synthesis of exfoliated two-dimensional polymers using hydrazone-linked covalent organic frameworks. *J. Am. Chem. Soc.* **2013**, *135*, 14952–14955.
[189] Li, X. X.; Goto, T.; Nomura, K.; Zhu, M. S.; Sekino, T.; Osakada, Y. Synthesis of porphyrin nanodisks from COFs through mechanical stirring and their photocatalytic activity. *Appl. Surf. Sci.* **2020**, *513*, 145720.
[190] Yusran, Y.; Li, H.; Guan, X. Y.; Li, D. H.; Tang, L. X.; Xue, M.; Zhuang, Z. B.; Yan, Y. S.; Valtchev, V.; Qiu, S. L. et al. Exfoliated mesoporous 2D covalent organic frameworks for high-rate electrochemical double-layer capacitors. *Adv. Mater.* **2020**, *32*, 1907289.
[191] Kang, Z. X.; Peng, Y. W.; Qian, Y. H.; Yuan, D. Q.; Addicoat, M. A.; Heine, T.; Hu, Z. G.; Tee, L.; Guo, Z. G.; Zhao, D. Mixed matrix membranes (MMMs) comprising exfoliated 2D covalent organic frameworks (COFs) for efficient CO_2 separation. *Chem. Mater.* **2016**, *28*, 1277–1285.
[192] Albacete, P.; López-Moreno, A.; Mena-Hernando, S.; Platero-Prats, A. E.; Pérez, E. M.; Zamora, F. Chemical sensing of water contaminants by a colloid of a fluorescent imine-linked covalent organic framework. *Chem. Commun.* **2019**, *55*, 1382–1385.
[193] Dong, J. Q.; Li, X.; Peh, S. B.; Yuan, Y. D.; Wang, Y. X.; Ji, D. X.; Peng, S. J.; Liu, G. L.; Ying, S. M.; Yuan, D. Q. et al. Restriction of molecular rotors in ultrathin two-dimensional covalent organic framework nanosheets for sensing signal amplification. *Chem. Mater.* **2019**, *31*, 146–160.
[194] Chen, X. D.; Li, Y. S.; Wang, L.; Xu, Y.; Nie, A. M.; Li, Q. Q.; Wu, F.; Sun, W. W.; Zhang, X.; Vajtai, R. et al. High-lithium-affinity chemically exfoliated 2D covalent organic frameworks. *Adv. Mater.* **2019**, *31*, 1901640.
[195] Mu, X. W.; Zhan, J. L.; Wang, J.; Cai, W.; Yuan, B. H.; Song, L.; Hu, Y. A novel and efficient strategy to exfoliation of covalent organic frameworks and a significant advantage of covalent organic frameworks nanosheets as polymer nano-enhancer: High interface compatibility. *J. Colloid Interface Sci.* **2019**, *539*, 609–618.
[196] Yao, J.; Liu, C.; Liu, X. Q.; Guo, J.; Zhang, S. B.; Zheng, J. F.; Li, S. H. Azobenzene-assisted exfoliation of 2D covalent organic frameworks into large-area, few-layer nanosheets for high flux and selective molecular separation membrane. *J. Membr. Sci.* **2020**, *601*, 117864.
[197] Mitra, S.; Kandambeth, S.; Biswal, B. P.; Khayum M, A.; Choudhury, C. K.; Mehta, M.; Kaur, G.; Banerjee, S.; Prabhune, A.; Verma, S. et al. Self-exfoliated guanidinium-based ionic covalent organic nanosheets (iCONs). *J. Am. Chem. Soc.* **2016**, *138*, 2823–2828.
[198] Chandra, S.; Kandambeth, S.; Biswal, B. P.; Lukose, B.; Kunjir, S.

M.; Chaudhary, M.; Babarao, R.; Heine, T.; Banerjee, R. Chemically stable multilayered covalent organic nanosheets from covalent organic frameworks via mechanical delamination. *J. Am. Chem. Soc.* **2013**, *135*, 17853–17861.

[199] Wang, L. L.; Zeng, C.; Xu, H.; Yin, P. C.; Chen, D. C.; Deng, J.; Li, M.; Zheng, N.; Gu, C.; Ma, Y. G. A highly soluble, crystalline covalent organic framework compatible with device implementation. *Chem. Sci.* **2019**, *10*, 1023–1028.

[200] Burke, D. W.; Sun, C.; Castano, I.; Flanders, N. C.; Evans, A. M.; Vitaku, E.; McLeod, D. C.; Lambeth, R. H.; Chen, L. X.; Gianneschi, N. C. et al. Acid exfoliation of imine-linked covalent organic frameworks enables solution processing into crystalline thin films. *Angew. Chem., Int. Ed.* **2020**, *59*, 5165–5171.

[201] Zhang, N.; Wang, T. S.; Wu, X.; Jiang, C.; Chen, F.; Bai, W.; Bai, R. K. Self-exfoliation of 2D covalent organic frameworks: Morphology transformation induced by solvent polarity. *RSC Adv.* **2018**, *8*, 3803–3808.

[202] Mal, A.; Mishra, R. K.; Praveen, V. K.; Khayum M, A.; Banerjee, R.; Ajayaghosh, A. Supramolecular reassembly of self-exfoliated ionic covalent organic nanosheets for label-free detection of double-stranded DNA. *Angew. Chem., Int. Ed.* **2018**, *57*, 8443–8447.

[203] Mal, A.; Vijayakumar, S.; Mishra, R. K.; Jacob, J.; Pillai, R. S.; Dileep Kumar, B. S.; Ajayaghosh, A. Supramolecular surface charge regulation in ionic covalent organic nanosheets: Reversible exfoliation and controlled bacterial growth. *Angew. Chem., Int. Ed.* **2020**, *59*, 8713–8719.

[204] Peng, Y. W.; Huang, Y.; Zhu, Y. H.; Chen, B.; Wang, L. Y.; Lai, Z. C.; Zhang, Z. C.; Zhao, M. T.; Tan, C. L.; Yang, N. L. et al. Ultrathin two-dimensional covalent organic framework nanosheets: Preparation and application in highly sensitive and selective DNA detection. *J. Am. Chem. Soc.* **2017**, *139*, 8698–8704.

[205] Haldar, S.; Roy, K.; Nandi, S.; Chakraborty, D.; Puthusseri, D.; Gawli, Y.; Ogale, S.; Vaidhyanathan, R. High and reversible lithium ion storage in self-exfoliated triazole-triformyl phloroglucinol-based covalent organic nanosheets. *Adv. Energy Mater.* **2018**, *8*, 1702170.

[206] Wang, M. D.; Quan, K. D.; Zheng, X. H.; Cao, Y.; Cui, X. Y.; Xue, M.; Pan, F. S. Facilitated transport membranes by incorporating self-exfoliated covalent organic nanosheets for CO_2/CH_4 separation. *Sep. Purif. Technol.* **2020**, *237*, 116457.

[207] Khayum M, A.; Kandambeth, S.; Mitra, S.; Nair, S. B.; Das, A.; Nagane, S. S.; Mukherjee, R.; Banerjee, R. Chemically delaminated free-standing ultrathin covalent organic nanosheets. *Angew. Chem., Int. Ed.* **2016**, *55*, 15604–15608.

[208] Haldar, S.; Roy, K.; Kushwaha, R.; Ogale, S.; Vaidhyanathan, R. Chemical exfoliation as a controlled route to enhance the anodic performance of COF in LIB. *Adv. Energy Mater.* **2019**, *9*, 1902428.

[209] Wang, S.; Wang, Q. Y.; Shao, P. P.; Han, Y. Z.; Gao, X.; Ma, L.; Yuan, S.; Ma, X. J.; Zhou, J. W.; Feng, X. et al. Exfoliation of covalent organic frameworks into few-layer redox-active nanosheets as cathode materials for lithium-ion batteries. *J. Am. Chem. Soc.* **2017**, *139*, 4258–4261.

[210] Ying, Y. P.; Tong, M. M.; Ning, S. C.; Ravi, S. K.; Peh, S. B.; Tan, S. C.; Pennycook, S. J.; Zhao, D. Ultrathin two-dimensional membranes assembled by ionic covalent organic nanosheets with reduced apertures for gas separation. *J. Am. Chem. Soc.* **2020**, *142*, 4472–4480.

[211] Liu, W. B.; Li, X. K.; Wang, C. M.; Pan, H. H.; Liu, W. P.; Wang, K.; Zeng, Q. D.; Wang, R. M.; Jiang, J. Z. A scalable general synthetic approach toward ultrathin imine-linked two-dimensional covalent organic framework nanosheets for photocatalytic CO_2 reduction. *J. Am. Chem. Soc.* **2019**, *141*, 17431–17440.

[212] Cheng, Y. D.; Ravi, S. K.; Wang, Y. X.; Tao, J. F.; Gu, Y. D.; Tan, S. C.; Zhao, D. Covalent organic nanosheets with large lateral size and high aspect ratio synthesized by Langmuir–Blodgett method. *Chin. Chem. Lett.* **2018**, *29*, 869–872.

[213] Tang, C.; Zheng, Y.; Jaroniec, M.; Qiao, S. Z. Electrocatalytic refinery for sustainable production of fuels and chemicals. *Angew. Chem., Int. Ed.* **2021**, *60*, 19572–19590.

[214] Wang, D. G.; Qiu, T. J.; Guo, W. H.; Liang, Z. B.; Tabassum, H.; Xia, D. G.; Zou, R. Q. Covalent organic framework-based materials for energy applications. *Energy Environ. Sci.* **2021**, *14*, 688–728.

[215] Tan, X. Y.; Yu, C.; Ren, Y. W.; Cui, S.; Li, W. B.; Qiu, J. S. Recent advances in innovative strategies for the CO_2 electroreduction reaction. *Energy Environ. Sci.* **2021**, *14*, 765–780.

[216] Wu, Q.; Xie, R. K.; Mao, M. J.; Chai, G. L.; Yi, J. D.; Zhao, S. S.; Huang, Y. B.; Cao, R. Integration of strong electron transporter tetrathiafulvalene into metalloporphyrin-based covalent organic framework for highly efficient electroreduction of CO_2. *ACS Energy Lett.* **2020**, *5*, 1005–1012.

[217] Morlanés, N.; Takanabe, K.; Rodionov, V. Simultaneous reduction of CO_2 and splitting of H_2O by a single immobilized cobalt phthalocyanine electrocatalyst. *ACS Catal.* **2016**, *6*, 3092–3095.

[218] Zhang, X.; Wu, Z. S.; Zhang, X.; Li, L. W.; Li, Y. Y.; Xu, H. M.; Li, X. X.; Yu, X. L.; Zhang, Z. S.; Liang, Y. Y. et al. Highly selective and active CO_2 reduction electrocatalysts based on cobalt phthalocyanine/carbon nanotube hybrid structures. *Nat. Commun.* **2017**, *8*, 14675.

[219] Lu, Y.; Zhang, J.; Wei, W. B.; Ma, D. D.; Wu, X. T.; Zhu, Q. L. Efficient carbon dioxide electroreduction over ultrathin covalent organic framework nanolayers with isolated cobalt porphyrin units. *ACS Appl. Mater. Interfaces* **2020**, *12*, 37986–37992.

[220] Maiti, S.; Chowdhury, A. R.; Das, A. K. Electrochemically facile hydrogen evolution using ruthenium encapsulated two dimensional covalent organic framework (2D COF). *ChemNanoMat* **2020**, *6*, 99–106.

[221] Yang, C.; Tao, S. S.; Huang, N.; Zhang, X. B.; Duan, J. G.; Makiura, R.; Maenosono, S. Heteroatom-doped carbon electrocatalysts derived from nanoporous two-dimensional covalent organic frameworks for oxygen reduction and hydrogen evolution. *ACS Appl. Nano Mater.* **2020**, *3*, 5481–5488.

[222] Mondal, S.; Mohanty, B.; Nurhuda, M.; Dalapati, S.; Jana, R.; Addicoat, M.; Datta, A.; Jena, B. K.; Bhaumik, A. A thiadiazole-based covalent organic framework: A metal-free electrocatalyst toward oxygen evolution reaction. *ACS Catal.* **2020**, *10*, 5623–5630.

[223] Nandi, S.; Singh, S. K.; Mullangi, D.; Illathvalappil, R.; George, L.; Vinod, C. P.; Kurungot, S.; Vaidhyanathan, R. Low band gap benzimidazole COF supported Ni_3N as highly active OER catalyst. *Adv. Energy Mater.* **2016**, *6*, 1601189.

[224] Niu, H. T.; Xia, C. F.; Huang, L.; Zaman, S.; Maiyalagan, T.; Guo, W.; You, B.; Xia, B. Y. Rational design and synthesis of one-dimensional platinum-based nanostructures for oxygen-reduction electrocatalysis. *Chin. J. Catal.* **2022**, *43*, 1459–1472.

[225] Jia, Y.; Zhang, L. Z.; Zhuang, L. Z.; Liu, H. L.; Yan, X. C.; Wang, X.; Liu, J. D.; Wang, J. C.; Zheng, Y. R.; Xiao, Z. H. et al. Identification of active sites for acidic oxygen reduction on carbon catalysts with and without nitrogen doping. *Nat. Catal.* **2019**, *2*, 688–695.

[226] Xu, Q.; Tang, Y. P.; Zhang, X. B.; Oshima, Y.; Chen, Q. H.; Jiang, D. L. Template conversion of covalent organic frameworks into 2D conducting nanocarbons for catalyzing oxygen reduction reaction. *Adv. Mater.* **2018**, *30*, 1706330.

[227] Liu, C.; Liu, F.; Li, H.; Chen, J. S.; Fei, J. Y.; Yu, Z. X.; Yuan, Z. W.; Wang, C. J.; Zheng, H. L.; Liu, Z. W. et al. One-Dimensional van der Waals heterostructures as efficient metal-free oxygen electrocatalysts. *ACS Nano* **2021**, *15*, 3309–3319.

[228] Yang, B.; Ding, W. L.; Zhang, H. H.; Zhang, S. J. Recent progress in electrochemical synthesis of ammonia from nitrogen: Strategies to improve the catalytic activity and selectivity. *Energy Environ. Sci.* **2021**, *14*, 672–687.

[229] Wang, C.; Zhao, Y. N.; Zhu, C. Y.; Zhang, M.; Geng, Y.; Li, Y. G.; Su, Z. M. A two-dimensional conductive Mo-based covalent organic framework as an efficient electrocatalyst for nitrogen fixation. *J. Mater. Chem. A* **2020**, *8*, 23599–23606.

[230] Wang, Z. F.; Yang, Y.; Zhao, Z. F.; Zhang, P. H.; Zhang, Y. S.; Liu, J. J.; Ma, S. Q.; Cheng, P.; Chen, Y.; Zhang, Z. J. Green synthesis of olefin-linked covalent organic frameworks for hydrogen fuel cell applications. *Nat. Commun.* **2021**, *12*, 1982.

[231] Wang, Z. F.; Zhu, Q. Q.; Wang, J. X.; Jin, F. Z.; Zhang, P. H.; Yan, D.; Cheng, P.; Chen, Y.; Zhang, Z. J. Industry-compatible covalent organic frameworks for green chemical engineering. *Sci. China*

Chem., in press, DOI: 10.1007/s11426-022-1391-0.

[232] Luo, Y. T.; Zhang, Z. Y.; Chhowalla, M.; Liu, B. L. Recent advances in design of electrocatalysts for high-current-density water splitting. *Adv. Mater.* **2022**, *34*, 2108133.

[233] Kibria, M. G.; Edwards, J. P.; Gabardo, C. M.; Dinh, C. T.; Seifitokaldani, A.; Sinton, D.; Sargent, E. H. Electrochemical CO_2 reduction into chemical feedstocks: From mechanistic electrocatalysis models to system design. *Adv. Mater.* **2019**, *31*, 1807166.

[234] Yang, D. R.; Wang, X. 2D π–conjugated metal–organic frameworks for CO_2 electroreduction. *SmartMat* **2022**, *3*, 54–67.

[235] Xu, Y. L.; Wang, C.; Huang, Y. H.; Fu, J. Recent advances in electrocatalysts for neutral and large-current-density water electrolysis. *Nano Energy* **2021**, *80*, 105545.

[236] Zhao, Q. L.; Wang, Y. A.; Li, M.; Zhu, S. Q.; Li, T. H.; Yang, J. X.; Lin, T.; Delmo, E. P.; Wang, Y. N.; Jang, J. et al. Organic frameworks confined Cu single atoms and nanoclusters for tandem electrocatalytic CO_2 reduction to methane. *SmartMat* **2022**, *3*, 183–193.

[237] Li, Z. X.; Guo, J.; Wan, Y.; Qin, Y. T.; Zhao, M. T. Combining metal–organic frameworks (MOFs) and covalent-organic frameworks (COFs): Emerging opportunities for new materials and applications. *Nano Res.* **2022**, *15*, 3514–3532.

[238] García-Arroyo, P.; Martínez-Periñán, E.; Cabrera-Trujillo, J. J.; Salagre, E.; Michel, E. G.; Martínez, J. I.; Lorenzo, E.; Segura, J. L. Pyrenetetraone-based covalent organic framework as an effective electrocatalyst for oxygen reduction reaction. *Nano Res.* **2022**, *15*, 3907–3912.